Generation of entangled-photon pairs from biexcitons in CuCl thin films: Nano-to-bulk crossover regime

Motoaki Bamba[1,*] and Hajime Ishihara[2]

[1]*Department of Materials Engineering Science, Osaka University, Toyonaka, Osaka 560-8531, Japan*

[2]*Department of Physics and Electronics, Osaka Prefecture University, Sakai, Osaka 599-8531, Japan*

(Received 3 April 2011; revised manuscript received 13 May 2011; published 18 July 2011)

We have constructed a theoretical framework of biexciton-resonant hyperparametric scattering for pursuit of high-power and high-quality generation of entangled-photon pairs. Our framework is applicable to the nano-to-bulk crossover regime where the center-of-mass motions of excitons and biexcitons are confined and material surroundings and the polarization correlation of generated photons can be considered. We have analyzed the generation of ultraviolet entangled photons from CuCl film with and without dielectric microcavity and revealed that in the nano-to-bulk crossover regime we generally get a high performance from the viewpoint of statistical accuracy and the generation efficiency can be enhanced by the optical cavity while maintaining the high performance. The nano-to-bulk crossover regime has a variety of degrees of freedom to control the entangled-photon generation, and the scattering spectra explicitly reflect quantized exciton-photon coupled modes in finite structures.

DOI: 10.1103/PhysRevB.84.045125 PACS number(s): 42.65.Lm, 42.50.Nn, 71.35.−y, 71.36.+c

I. INTRODUCTION

Entangled-photon pairs have been discussed in relation with the Einstein-Padolsky-Rosen (EPR) paradox,[1] and nowadays they play an important role in quantum-information technologies. The pursuit of high-quality and high-efficiency generation of entangled photons is a fascinating subject in the fields of quantum optics and solid-state physics. In addition to the standard generation method by parametric down-conversion (PDC) in second-order nonlinear crystals,[2,3] the generation scheme using single semiconductor quantum dots[4–8] attracts much attention, because single pairs of entangled photons are generated in principle from a single dot, and it can be a deterministic source of entangled pairs. Recently, the generation efficiency is highly enhanced by implementing an optical cavity by distributed Bragg reflectors (DBRs)[6] and also by molecule of micropillars.[8] Further, the entangled-photon generation by current injection has been reported.[7] On the other hand, the entangled-photon pairs are also considered as an excitation light source, and it is of growing importance for the next-generation technologies of fabrication and chemical reaction.[9] For this purpose, it is essential to generate high-power and high-quality entangled-photon beams, and this high-power but probabilistic generation is another direction of research in addition to the deterministic generation by single quantum dots.

In the process of PDC,[2,3] an incident photon with frequency $\omega_{\rm in}$ and wave number $\boldsymbol{k}_{\rm in}$ splits into two photons $(\omega_1,\boldsymbol{k}_1)$ and $(\omega_2,\boldsymbol{k}_2)$ satisfying the conservations of energy $\omega_{\rm in}=\omega_1+\omega_2$ and of wave vector $\boldsymbol{k}_{\rm in}=\boldsymbol{k}_1+\boldsymbol{k}_2$. This second-order nonlinear process creates polarization-correlated entangled-photon pairs in nonlinear optical crystals with birefringence. On the other hand, Savasta *et al.*[12] suggested and Edamatsu *et al.*[10] experimentally demonstrated that ultraviolet entangled-photon pairs are generated by biexciton-resonant hyperparametric scattering (RHPS) in CuCl (see Fig. 1). The RHPS is a third-order nonlinear process, in which two incident photons resonantly create a biexciton (excitonic molecule) with $(2\omega_{\rm in},2\boldsymbol{k}_{\rm in})$ and it spontaneously collapses into a photon pair satisfying $2\omega_{\rm in}=\omega_1+\omega_2$ and $2\boldsymbol{k}_{\rm in}=\boldsymbol{k}_1+\boldsymbol{k}_2$. Since the lowest level of biexcitons in CuCl, which was resonantly excited in the experiment, has zero angular momentum,[11] the emitted pair consists of left- and right-circularly polarized photons conserving the total angular momentum. Owing to the two possible decay paths through exciton-polariton branches, the polarizations of emitted photons are entangled.

The generation efficiency of RHPS is quite high compared to that of PDC, because of the giant oscillator strength of the two-photon absorption involving the biexcitons in CuCl.[11] However, in the first experimental report,[10] a part of detected pairs has no entanglement, and this noise was subtracted in the estimation of entanglement of the generated pairs. As indicated by Oohata *et al.*,[13] the main contribution of the unentangled pairs is the accidental collapse of two biexcitons, and this problem has been successfully suppressed by using high-repetition and weak-power laser pulses, because the number of unentangled pairs (noise) is increased by $I_{\rm in}{}^4$ for increasing the pumping power $I_{\rm in}$ while the number of entangled pairs (signal) is proportional to $I_{\rm in}{}^2$. However, this fundamental trade-off problem between signal intensity and S/N ratio should be resolved from the viewpoint of material structures[14] in addition to the improvement of pumping condition in Ref. 13. While one solution is using single quantum dots as deterministic sources,[4–8] for the pursuit of high-power generation there is a proposal of using an optical cavity embedding an excitonic quantum well for the improvement of generation efficiency.[15,16] Furthermore, owing to the rapid radiative decay by the exciton superradiance (enhancement of interaction volume between excitons and photons),[17,18] we have theoretically revealed that the trade-off problem can be resolved by simultaneously realizing a high generation efficiency and a rapid radiative decay rate of excitons, which are achieved by a DBR cavity embedding an excitonic nanolayer in the nano-to-bulk crossover regime.[14]

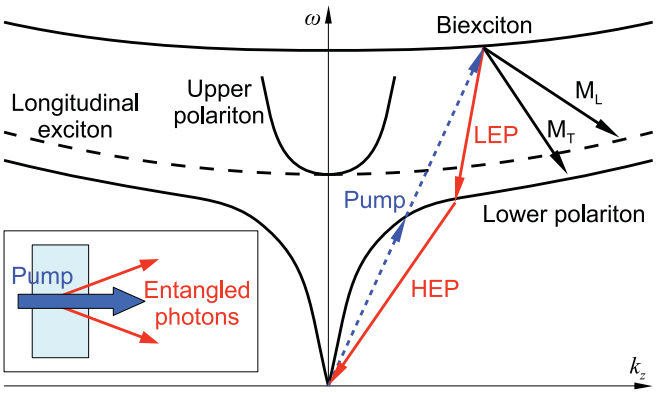

FIG. 1. (Color online) The biexciton-resonant hyperparametric scattering (RHPS) is depicted on biexciton, exciton-polariton, and longitudinal exciton dispersion curves. Biexcitons are resonantly created by two-photon absorption, and entangled-photon pairs are emitted when the biexcitons decay into the lower exciton-polariton branch. This emission appears in the scattering spectrum as two peaks called LEP and HEP (lower and higher energy polaritons) as seen in Fig. 3. Due to the conservation of energy and of wave vectors, the positions of the two peaks depend on scattering angle,[10,11] and the entangled two photons are emitted symmetrically about the pump beam as shown in the inset. Two additional peaks called M_T and M_L in scattering spectra originate from the biexciton decay into transverse and longitudinal exciton levels, respectively.

In a microcrystal, such as a quantum dot and quantum well smaller than the Bohr radius of excitons, the electron and hole are individually confined in the crystal, and the relative motion of excitons and also the binding energy are strongly modified from those in bulk crystal. When the crystal size is larger than the exciton Bohr radius but small enough compared to the light wavelength, the center-of-mass motion of excitons is confined, and the center-of-mass kinetic energy is quantized.[19,20] When the crystal size is comparable or a few times larger than the wavelength (nano-to-bulk crossover regime), the system is characterized by exciton-photon coupled modes with peculiar resonance energies and radiative lifetimes, and the coupled modes are gradually reduced to bulk polariton branches by the increase of crystal size.[18,21–25] In this crossover regime, due to the center-of-mass confinement of excitons and the spatially resonant coupling with electromagnetic fields, the system shows a variety of optical responses compared to bulk materials and also to quantum dots. Owing to the recent development of nanoscale fabrication, anomalous nonlinear optical responses have been reported in semiconductor nanostructures and in the nano-to-bulk crossover regime.[17,26–36] Further, in such regime, we obtain rapid radiative decay rates of excitons on the order of 100 fs due to the exciton superradiance.[17] Concerning the entangled-photon generation, while the performance of the PDC method is almost governed by the choice of nonlinear materials and its thickness, the RHPS method significantly depends on the quantum states of excitons and biexcitons, because it is a resonant process involving elementary excitations. In the nano-to-bulk crossover regime, the generation of entangled photon pairs by RHPS is qualitatively modified with respect to frequencies, angles, polarizations, and phase difference of the generated entangled state as discussed in our previous Letter.[14] In the present paper, we will show in detail our theoretical framework for the investigation of the entangled-photon generation in the nano-to-bulk crossover regime with multilayer structures, especially an excitonic layer embedded in DBR cavity.

We explain our theoretical framework in Sec. II, and show in detail the way to calculate the one-photon scattering intensity and the two-photon coincidence intensity of RHPS in the case of multilayer structure in Sec. III. The calculated results are shown in Sec. IV, and the discussion is summarized in Sec. V.

II. THEORETICAL FRAMEWORK

The emission spectra from Bose-Einstein condensation of biexcitons were calculated by Inoue and Hanamura,[37] and these authors also investigated the relation between energies and scattering angles of two peaks called LEP and HEP (lower and higher energy polaritons; see Fig. 1). Later, Hanamura and Takagahara[38] calculated line shapes of the so-called M_T and M_L peaks, which are emitted by the relaxations of biexcitons to transverse and longitudinal excitons, respectively. The entanglement of the scattered photons by RHPS was first pointed out by Savasta *et al.*,[12] and their theoretical framework[39] is based on the quantum electrodynamics (QED) theory for dispersive and absorbing media[40,41] and on the exciton-exciton correlation functions calculated from first principles.[42,43]

In the present paper, in order to correctly treat the center-of-mass confinement of excitons, we construct our framework by extending the QED theory of excitons,[44] which simultaneously solves the equation of motion of excitons and of electromagnetic fields inheriting the concepts of the above QED theories[40,41] and of the semiclassical nonlocal theory[30,45] (or the so-called ABC-free theory[46]). It is well known that the center-of-mass motion of excitons raises more than one propagating modes of exciton-polaritons in their band gap, and the RHPS process has been used to observe the dispersion of polaritons[11,37,47–49] and also to measure the translational masses of excitons and biexcitons.[11,50–52] Moreover, optical responses explicitly reflect the confinement of center-of-mass motion of excitons in nanostructured materials and also in the nano-to-bulk crossover regime,[17–20,26–36] on which we focus in the present paper.

Concerning the treatment of biexcitons, we suppose the excitons as pure bosons and consider an exciton-exciton interaction leading to the creation of biexcitons. However, instead of the detailed treatment in the theory of Savasta *et al.*,[39] we simply represent the relative motion of the lowest level of biexcitons with some parameters measured in experiments,[11,53,54] and the coefficients of the exciton-exciton interaction is replaced by the assumed wave function and the binding energy of biexcitons. This treatment is very simple and useful to catch the behavior of biexciton lowest level in CuCl even in the nano-to-bulk crossover regime, because the exciton and biexciton states in CuCl has been well analyzed by the bipolariton theory[55,56] and RHPS experiments.[54,57,58] While the treatment of biexcitons is in general a four-body problem with two electrons and two holes and it is usually hard to solve; owing to the above-mentioned simple treatment, we can easily discuss the polarization correlation of photon pairs

emitted from the biexciton lowest level, which has no angular momentum.

Moreover, by using the dyadic Green's function for the wave equation of the electric field, we can consider the surroundings of excitonic material, such as an optical cavity consisting of two DBRs. In order to extract the scattering fields, instead of using the input-output relation,[41,59–63] we consider the definition of the Green's function and commutation relations of fluctuation operators. This simple treatment is valid at least in multilayer systems and useful to consider complicated structures.

In the following subsections, we show our theoretical framework to calculate the signal and noise intensities by RHPS. We show the Hamiltonian in Sec. II A, and the equations of motion are derived in Sec. II B. In order to discuss the RHPS, we use some approximations, which are explained in Sec. II C. The model of biexcitons is shown in Sec. II D. In order to solve the equations of motion, we use the Green's function technique explained in Sec. II E. Finally, we derive the expression of observables in Sec. II F.

A. Hamiltonian

Our theoretical framework is based on the QED theory of excitons.[44] The Hamiltonian is written as

$$\hat{H} = \hat{H}_{\rm ex} + \hat{H}_{\rm res} + \hat{H}_{\rm int} + \hat{H}_{\rm em}, \tag{1}$$

where $\hat{H}_{\rm ex}$ describes the excitonic system, $\hat{H}_{\rm res}$ represents a reservoir for the nonradiative damping of excitons, $\hat{H}_{\rm int}$ is the exciton-photon interaction, and $\hat{H}_{\rm em}$ describes the electromagnetic fields and a background dielectric medium as discussed in Ref. 64 and also used in Ref. 44. In order to discuss the biexciton-RHPS, we consider an exciton-exciton interaction with coefficient $V_{\mu,\nu;\mu',\nu'}$. Namely, the Hamiltonian of excitonic system is written as

$$\hat{H}_{\rm ex} = \sum_{\mu} \hbar\omega_{\mu} \hat{b}_{\mu}^{\dagger} \hat{b}_{\mu} + \frac{1}{2} \sum_{\mu,\mu',\nu,\nu'} V_{\mu,\nu;\mu',\nu'} \hat{b}_{\mu}^{\dagger} \hat{b}_{\nu}^{\dagger} \hat{b}_{\nu'} \hat{b}_{\mu'}, \tag{2}$$

where $\hat{b}_{\mu}$ is the annihilation operator of an exciton in state μ and ω_{μ} is its eigenfrequency. We treat the excitons as pure bosons satisfying

$$[\hat{b}_{\mu}, \hat{b}_{\mu'}^{\dagger}] = \delta_{\mu,\mu'}, \tag{3a}$$

$$[\hat{b}_{\mu}, \hat{b}_{\mu'}] = 0, \tag{3b}$$

and their nonbosonic behavior is described by the exciton-exciton interaction, the second term in Eq. (2). The reservoir $\hat{H}_{\rm res}$ is written as

$$\hat{H}_{\rm res} = \sum_{\mu} \int_0^{\infty} d\Omega \{\hbar\Omega \hat{d}_{\mu}^{\dagger}(\Omega) \hat{d}_{\mu}(\Omega) + [\hat{b}_{\mu} + \hat{b}_{\mu}^{\dagger}][g_{\mu}(\Omega) \hat{d}_{\mu}(\Omega) + g_{\mu}^{*}(\Omega) \hat{d}_{\mu}^{\dagger}(\Omega)]\}, \tag{4}$$

where $\hat{d}_{\mu}(\Omega)$ is the annihilation operator of harmonic oscillator with frequency Ω interacting with excitons in state μ and $g_{\mu}(\Omega)$ is the coupling coefficient. The oscillators are independent of each other and satisfy the following commutation relations:

$$[\hat{d}_{\mu}(\Omega), \hat{d}_{\mu'}^{\dagger}(\Omega')] = \delta_{\mu,\mu'} \delta(\Omega - \Omega'), \tag{5a}$$

$$[\hat{d}_{\mu}(\Omega), \hat{d}_{\mu'}(\Omega')] = 0. \tag{5b}$$

Further, $\hat{H}_{\rm int}$ is simply written as a product of electric field $\hat{\boldsymbol{E}}(\boldsymbol{r})$ and excitonic polarization $\hat{\boldsymbol{P}}_{\rm ex}(\boldsymbol{r})$:

$$\hat{H}_{\rm int} = -\int d\boldsymbol{r}\ \hat{\boldsymbol{P}}_{\rm ex}(\boldsymbol{r}) \cdot \hat{\boldsymbol{E}}(\boldsymbol{r}). \tag{6}$$

The excitonic polarization is represented as

$$\hat{\boldsymbol{P}}_{\rm ex}(\boldsymbol{r}) = \sum_{\mu} \boldsymbol{\mathcal{P}}_{\mu}(\boldsymbol{r}) \hat{b}_{\mu} + {\rm H.c.}, \tag{7}$$

where the coefficient $\boldsymbol{\mathcal{P}}_{\mu}(\boldsymbol{r})$ is expressed by the exciton center-of-mass wave function $g_{\mu}^{\rm ex}(\boldsymbol{r})$ and unit vector $\boldsymbol{e}_{\mu}$ in polarization direction as

$$\boldsymbol{\mathcal{P}}_{\mu}(\boldsymbol{r}) = M \boldsymbol{e}_{\mu} g_{\mu}^{\rm ex}(\boldsymbol{r}). \tag{8}$$

The absolute value of M can be evaluated by the longitudinal-transverse (LT) splitting energy $\Delta_{\rm LT} = |M|^2/\varepsilon_0 \varepsilon_{\rm bg}^{\rm ex}$ of excitons, the vacuum permittivity ε_0, and the background dielectric constant $\varepsilon_{\rm bg}^{\rm ex}$ of the excitonic medium.

B. Equations of motion

According to Ref. 44 or the QED theories of dispersive and absorbing media,[40,41,64] the equation of motion of electric field $\hat{\boldsymbol{E}}(\boldsymbol{r})$ is derived in frequency domain as

$$\nabla \times \nabla \times \check{\boldsymbol{E}}^{+}(\boldsymbol{r},\omega) - \frac{\omega^2}{c^2} \varepsilon_{\rm bg}(\boldsymbol{r},\omega) \check{\boldsymbol{E}}^{+}(\boldsymbol{r},\omega) = i\mu_0\omega \check{\boldsymbol{J}}_0(\boldsymbol{r},\omega) + \mu_0\omega^2 \check{\boldsymbol{P}}_{\rm ex}^{+}(\boldsymbol{r},\omega). \tag{9}$$

Here, μ_0 is the vacuum permeability and $\varepsilon_{\rm bg}(\boldsymbol{r},\omega)$ is the dielectric function of the background medium with arbitrary three-dimensional structure. We write an operator with a check ($\check{}$) in the frequency domain. $\check{\boldsymbol{J}}_0(\boldsymbol{r},\omega)$ describes the fluctuation of electromagnetic fields and satisfies

$$\begin{aligned}[\check{\boldsymbol{J}}_0(\boldsymbol{r},\omega), \{\check{\boldsymbol{J}}_0(\boldsymbol{r}',\omega'^{*})\}^{\dagger}] &= [\check{\boldsymbol{J}}_0(\boldsymbol{r},\omega), \check{\boldsymbol{J}}_0(\boldsymbol{r}', -\omega')] \\ &= \delta(\omega - \omega')\delta(\boldsymbol{r} - \boldsymbol{r}') \frac{\varepsilon_0 \hbar\omega^2}{\pi} {\rm Im}[\varepsilon_{\rm bg}(\boldsymbol{r},\omega)] \overleftrightarrow{\mathbf{1}}\,.\end{aligned} \tag{10}$$

In the same manner as in Ref. 44, we obtain the equation of excitons' motion in frequency domain as

$$\begin{aligned}[\hbar\omega_{\mu} - \hbar\omega - i\gamma_{\rm ex}/2] \check{b}_{\mu}(\omega) &= \int d\boldsymbol{r}\ \boldsymbol{\mathcal{P}}_{\mu}^{*}(\boldsymbol{r}) \cdot \check{\boldsymbol{E}}^{+}(\boldsymbol{r},\omega) + \check{\mathcal{D}}_{\mu}(\omega) \\ &\quad - \sum_{\nu} \sum_{\mu',\nu'} V_{\mu,\nu;\mu',\nu'} \int_{-\infty}^{\infty} dt\ \frac{e^{i\omega t}}{2\pi} \hat{b}_{\nu}^{\dagger}(t) \hat{b}_{\nu'}(t) \hat{b}_{\mu'}(t),\end{aligned} \tag{11}$$

where $\gamma_{\rm ex}$ is the nonradiative damping width defined in terms of $\{g_{\mu}(\Omega)\}$ as shown in Eq. (D7) of Ref. 44, and $\check{\mathcal{D}}_{\mu}(\omega)$ represents the fluctuation by the damping satisfying

$$\begin{aligned}[\check{\mathcal{D}}_{\mu}(\omega), \{\check{\mathcal{D}}_{\mu'}(\omega'^{*})\}^{\dagger}] &= [\check{\mathcal{D}}_{\mu}(\omega), \check{\mathcal{D}}_{\mu'}(-\omega')] \\ &= \delta_{\mu,\mu'} \delta(\omega - \omega') \frac{\hbar\gamma_{\rm ex}}{2\pi}.\end{aligned} \tag{12}$$

The last term on the right-hand side of Eq. (11) is the nonlinear term due to the exciton-exciton interaction.

Here, we define a new operator

$$\hat{B}_\lambda \equiv \frac{1}{2}\sum_{\mu,\nu} F^*_{\lambda,\mu,\nu}\hat{b}_\nu\hat{b}_\mu, \tag{13}$$

which annihilates a biexciton (excitonic molecule) in state λ and describes a two-exciton eigenstate $\hat{B}^\dagger_\lambda|\mathrm{g}\rangle$ by applying it to the ground state $|\mathrm{g}\rangle$ of matter system. The coefficient $F_{\lambda,\mu,\nu}$ is invariant by the exchange of two exciton indices as

$$F_{\lambda,\mu,\nu} = F_{\lambda,\nu,\mu}. \tag{14}$$

Further, it is orthonormal,

$$\frac{1}{2}\sum_{\mu,\nu} F_{\lambda,\mu,\nu}F^*_{\lambda',\mu,\nu} = \delta_{\lambda,\lambda'}, \tag{15}$$

and also has a completeness

$$\sum_{\lambda} F_{\lambda,\mu,\nu}F^*_{\lambda,\mu',\nu'} = \delta_{\mu,\mu'}\delta_{\nu,\nu'} + \delta_{\mu,\nu'}\delta_{\nu,\mu'}. \tag{16}$$

From the excitonic Hamiltonian $\hat{H}_{\mathrm{ex}}$ [Eq. (2)], the coefficient $F_{\lambda,\mu,\nu}$ and eigenfrequency Ω_λ of biexciton eigenstate λ should satisfy

$$(\hbar\omega_\mu + \hbar\omega_\nu)F_{\lambda,\mu,\nu} + \sum_{\mu',\nu'} V_{\mu,\nu;\mu',\nu'}F_{\lambda,\mu',\nu'} = \hbar\Omega_\lambda F_{\lambda,\mu,\nu}. \tag{17}$$

By using Eqs. (14) and (16), we can rewrite Eq. (13) as

$$\sum_{\lambda} F_{\lambda,\mu,\nu}\hat{B}_\lambda = \hat{b}_\nu\hat{b}_\mu. \tag{18}$$

Therefore, from this relation and Eq. (17), we can rewrite Eq. (11) as

$$\begin{aligned}&[\hbar\omega_\mu - \hbar\omega - i\gamma_{\mathrm{ex}}/2]\check{b}_\mu(\omega)\\ &= \int d\boldsymbol{r}\ \boldsymbol{\mathcal{P}}^*_\mu(\boldsymbol{r})\cdot\check{\boldsymbol{E}}^+(\boldsymbol{r},\omega) + \check{\mathcal{D}}_\mu(\omega)\\ &\quad + \sum_{\lambda,\nu}(\hbar\omega_\mu + \hbar\omega_\nu - \hbar\Omega_\lambda)F_{\lambda,\mu,\nu}\\ &\quad \times \int_{-\infty}^{\infty} d\omega'\{\check{b}_\nu(\omega'-\omega)\}^\dagger\check{B}_\lambda(\omega').\end{aligned} \tag{19}$$

On the other hand, by deriving the equation of motion for $\hat{B}_\lambda$ and by using the above relations, we get

$$\begin{aligned}&(\hbar\Omega_\lambda - \hbar\omega)\check{B}_\lambda(\omega)\\ &= \sum_{\mu,\nu} F^*_{\lambda,\mu,\nu}\int_{-\infty}^{\infty} d\omega'(\hbar\omega_\nu - \hbar\omega')\check{b}_\nu(\omega')\check{b}_\mu(\omega-\omega').\end{aligned} \tag{20}$$

In principle, the biexciton RHPS process is described by the three equations of motion (9), (19), and (20), and commutation relations (10) and (12). However, in the actual calculation, we use the following approximation.

C. Approximation for RHPS process

We suppose that a coherent light beam resonantly excites biexcitons and their amplitude is large enough compared to the vacuum fluctuation. In this situation, if we do not consider the higher order processes, the biexciton operator in the nonlinear term of Eq. (19) can be replaced by the amplitude $\mathcal{B}_\lambda(\omega') = \langle\check{B}_\lambda(\omega')\rangle$. Further, we replace $\check{b}_\nu(\omega'-\omega)$ in the nonlinear term by $\check{b}^{(1)}_\nu(\omega'-\omega)$, which satisfies the linear equation

$$\begin{aligned}&[\hbar\omega_\mu - \hbar\omega - i\gamma_{\mathrm{ex}}/2]\check{b}^{(1)}_\mu(\omega)\\ &= \int d\boldsymbol{r}\ \boldsymbol{\mathcal{P}}^*_\mu(\boldsymbol{r})\cdot\check{\boldsymbol{E}}^+(\boldsymbol{r},\omega) + \check{\mathcal{D}}_\mu(\omega).\end{aligned} \tag{21}$$

Simultaneously solving this equation and Eq. (9), $\check{b}^{(1)}_\mu(\omega)$ can be expressed by the fluctuation operators $\check{\boldsymbol{J}}_0(\boldsymbol{r},\omega)$ and $\check{\mathcal{D}}_\mu(\omega)$. The calculation is straightforward by using the Green's function technique as will be shown in Sec. II E. Under the above approximation, Eq. (19) is rewritten as

$$\begin{aligned}&[\hbar\omega_\mu - \hbar\omega - i\gamma_{\mathrm{ex}}/2]\check{b}_\mu(\omega)\\ &\simeq \int d\boldsymbol{r}\ \boldsymbol{\mathcal{P}}^*_\mu(\boldsymbol{r})\cdot\check{\boldsymbol{E}}^+(\boldsymbol{r},\omega) + \check{\mathcal{D}}_\mu(\omega)\\ &\quad + \sum_{\lambda,\nu}(\hbar\omega_\mu + \hbar\omega_\nu - \hbar\Omega_\lambda)F_{\lambda,\mu,\nu}\\ &\quad \times \int_{-\infty}^{\infty} d\omega'\{\check{b}^{(1)}_\nu(\omega'-\omega)\}^\dagger\mathcal{B}_\lambda(\omega').\end{aligned} \tag{22}$$

By solving this equation and Eq. (9), we can represent $\check{\boldsymbol{E}}^+(\boldsymbol{r},\omega)$ by the fluctuation operators $\check{\boldsymbol{J}}_0(\boldsymbol{r},\omega)$ and $\check{\mathcal{D}}_\mu(\omega)$. This calculation is also straightforward by using the Green's function.

For the calculation of $\mathcal{B}_\lambda(\omega)$, we suppose that the biexciton amplitude is not decreased by the scattering, because its contribution is small compared to the pumping light. Under this approximation, by phenomenologically introducing a damping constant γ_{bx}, the biexciton amplitude is obtained from Eq. (20) as

$$\begin{aligned}\mathcal{B}_\lambda(\omega) &\simeq \frac{1}{\hbar\Omega_\lambda - \hbar\omega - i\gamma_{\mathrm{bx}}/2}\sum_{\mu,\nu} F^*_{\lambda,\mu,\nu}\\ &\quad \times \int_{-\infty}^{\infty} d\omega'\ (\hbar\omega_\nu - \hbar\omega')\langle\check{b}^{(1)}_\nu(\omega')\rangle\langle\check{b}^{(1)}_\mu(\omega-\omega')\rangle,\end{aligned} \tag{23}$$

where $\langle\check{b}^{(1)}_\nu(\omega')\rangle$ can be calculated from Eqs. (9) and (21) by considering an incident light beam as a homogeneous solution of Eq. (9). Under the weak bipolariton regime,[16] where the coupling between exciton-polariton and biexciton is small enough compared to their broadening, the approximated expression (23) of biexciton amplitude is sufficient for the discussion of RHPS process. While Savasta *et al.* considered the equation of motion of projection operators,[12,39] they also used a similar approximation for the treatment of biexcitons under the detailed verification of its validity.

D. Model of biexcitons

Although $F_{\lambda,\mu,\nu}$ and Ω_λ should be in principle determined from Eq. (17) for given nonlinear coefficients $\{V_{\mu,\nu;\mu',\nu'}\}$, we instead express $F_{\lambda,\mu,\nu}$ and Ω_λ by using experimental results. This treatment is useful because we already know many parameters of the lowest level of biexcitons in CuCl by longstanding experimental and theoretical studies.[11]

It is well known that the lowest level of biexcitons in CuCl is the singlet and has zero angular momentum, because of the exchange interactions between two electrons and between two holes.[11] Since we suppose the resonant two-photon excitation of the lowest level, we only consider the lowest relative motion of biexciton in our calculation. Further, according to the RHPS experiments in Ref. 54, the lowest biexciton state mainly consists of $1s$ excitons, and the contribution from the higher exciton states was estimated on the order of 10^{-4}. Therefore, we consider only $1s$ relative motion of excitons, which has a degree of freedom of polarization direction $\xi_\mu = \{x,y,z\}$. The relative motions of excitons and biexcitons are approximately treated as those in bulk CuCl.[11] The lowest biexciton level $|J=0,M=0\rangle_{\rm bx}$ with zero angular momentum is represented as

$$|J=0,M=0\rangle_{\rm bx} = \tfrac{1}{2}\{|0,0;0,0\rangle_{\rm 2ex} + |1,1;1,-1\rangle_{\rm 2ex} + |1,-1;1,1\rangle_{\rm 2ex} - |1,0;1,0\rangle_{\rm 2ex}\}, \quad (24)$$

where $|j_1,m_1;j_2,m_2\rangle_{\rm 2ex}$ is the two-exciton state represented in terms of angular momenta (j_1,m_1) and (j_2,m_2) of two excitons. This expression surely reflects the polarization correlation of photon pairs observed in RHPS experiments[10,13] and also determines the phase between the two states:

$$\Phi_+ = (|L,R\rangle + |R,L\rangle)/\sqrt{2} \quad (25a)$$

$$= (|H,H\rangle + |V,V\rangle)/\sqrt{2}. \quad (25b)$$

Here, $|L,R\rangle$ means that one photon is left- and the other is right-circularly polarized, and $|R,L\rangle$ is the opposite state. $|H,H\rangle$ and $|V,V\rangle$ respectively mean that both photons are horizontally and vertically polarized. By rewriting each exciton state in terms of the polarization direction as

$$|j,m\rangle = \begin{cases} |1,1\rangle = -(|x\rangle + i|y\rangle)/\sqrt{2}, \\ |1,0\rangle = |z\rangle, \\ |1,-1\rangle = (|x\rangle - i|y\rangle)/\sqrt{2}, \end{cases} \quad (26)$$

Eq. (24) is rewritten as

$$|J=0,M=0\rangle_{\rm bx} = \tfrac{1}{2}\{|0,0;0,0\rangle_{\rm 2ex} - |x;x\rangle_{\rm 2ex} - |y;y\rangle_{\rm 2ex} - |z;z\rangle_{\rm 2ex}\}, \quad (27)$$

which also reflects the polarization correlation (25b).

Considering the relative motion $\Psi(\boldsymbol{r})$ of two excitons in the lowest biexciton level, the coefficient is written as

$$F_{\lambda,\mu,\nu} = \delta_{\lambda,\mu,\nu}\int d\boldsymbol{r}\int d\boldsymbol{r}'\ \Psi(\boldsymbol{r}')g_\lambda^{\rm bx}(\boldsymbol{r})g_\mu^{\rm ex*}(\boldsymbol{r}+\boldsymbol{r}')g_\nu^{\rm ex*}(\boldsymbol{r}), \quad (28)$$

where $g_m^{\rm ex}(\boldsymbol{r})$ and $g_l^{\rm bx}(\boldsymbol{r})$ are center-of-mass wave functions of excitons and biexcitons, respectively, and

$$\delta_{\lambda,\mu,\nu} = \delta_{\xi_\mu,\xi_\nu} \quad (29)$$

represents the polarization selection rule reflecting the lowest biexciton level [Eq. (27)]. Here, we suppose that the Bohr radius of the biexciton (1.5 nm in CuCl)[65] is much smaller than the crystal size, and the relative motion of biexcitons is not strongly modified from the bulk one. Namely, we approximate the above expression as

$$F_{\lambda,\mu,\nu} \simeq \delta_{\lambda,\mu,\nu}\Phi\int d\boldsymbol{r}\ g_\lambda^{\rm bx}(\boldsymbol{r})\ g_\mu^{\rm ex*}(\boldsymbol{r})\ g_\nu^{\rm ex*}(\boldsymbol{r}). \quad (30)$$

Here, Φ is defined as

$$\Phi \equiv \int d\boldsymbol{r}\ \Psi(\boldsymbol{r}), \quad (31)$$

and $|\Phi|^2$ represents the effective volume of the lowest biexciton state. It was estimated by an experiment[53] and was also used as a parameter in theoretical work of Ref. 66.

E. Green's function technique

Next, we explain how we simultaneously solve the equation of motion of electric field [Eq. (9)] and that of excitons [Eq. (21) or Eq. (22)]. By using the dyadic Green's function satisfying

$$\nabla\times\nabla\times\overleftrightarrow{\mathsf{G}}(\boldsymbol{r},\boldsymbol{r}',\omega) - \frac{\omega^2}{c^2}\varepsilon_{\rm bg}(\boldsymbol{r},\omega)\overleftrightarrow{\mathsf{G}}(\boldsymbol{r},\boldsymbol{r}',\omega) = \delta(\boldsymbol{r}-\boldsymbol{r}')\overleftrightarrow{\mathbf{1}}, \quad (32)$$

we can rewrite Eq. (9) as

$$\check{\boldsymbol{E}}^+(\boldsymbol{r},\omega) = \check{\boldsymbol{E}}_0^+(\boldsymbol{r},\omega) + \mu_0\omega^2\int d\boldsymbol{r}'\ \overleftrightarrow{\mathsf{G}}(\boldsymbol{r},\boldsymbol{r}',\omega)\cdot\check{\boldsymbol{P}}_{\rm ex}^+(\boldsymbol{r}',\omega), \quad (33)$$

where $\check{\boldsymbol{E}}_0^+(\boldsymbol{r},\omega)$ represents the electric field in the background $(\hat{H}_{\rm em})$ system, and it is defined as

$$\check{\boldsymbol{E}}_0^+(\boldsymbol{r},\omega) \equiv i\mu_0\omega\int d\boldsymbol{r}'\ \overleftrightarrow{\mathsf{G}}(\boldsymbol{r},\boldsymbol{r}',\omega)\cdot\check{\boldsymbol{J}}_0(\boldsymbol{r}',\omega). \quad (34)$$

From Eq. (10), $\check{\boldsymbol{E}}_0^+(\boldsymbol{r},\omega)$ satisfies[44]

$$[\check{\boldsymbol{E}}_0^+(\boldsymbol{r},\omega),\check{\boldsymbol{E}}_0^-(\boldsymbol{r}',\omega')] = [\check{\boldsymbol{E}}_0^+(\boldsymbol{r},\omega),\check{\boldsymbol{E}}_0^+(\boldsymbol{r}',-\omega')] = \delta(\omega-\omega')\frac{\mu_0\hbar\omega^2}{i2\pi}[\overleftrightarrow{\mathsf{G}}(\boldsymbol{r},\boldsymbol{r}',\omega) - \overleftrightarrow{\mathsf{G}}^*(\boldsymbol{r},\boldsymbol{r}',\omega)]. \quad (35)$$

The expression of $\overleftrightarrow{\mathsf{G}}(\boldsymbol{r},\boldsymbol{r}',\omega)$ in a planar system (dielectric multilayer) is already known[67] and will be shown in Sec. III.

Substituting Eq. (33) into Eq. (22), we obtain a simultaneous equation set for exciton operators under the rotating-wave approximation (RWA) as

$$\sum_{\mu'} S_{\mu,\mu'}(\omega)\check{b}_{\mu'}(\omega) = \int d\boldsymbol{r}\ \boldsymbol{\mathcal{P}}_\mu^*(\boldsymbol{r})\cdot\check{\boldsymbol{E}}_0^+(\boldsymbol{r},\omega) + \check{\mathcal{D}}_\mu(\omega) + \sum_{\lambda,\nu}(\hbar\omega_\mu + \hbar\omega_\nu - \hbar\Omega_\lambda)F_{\lambda,\mu,\nu} \times\int_{-\infty}^{\infty}d\omega'\{\check{b}_\nu^{(1)}(\omega'-\omega)\}^\dagger\mathcal{B}_\lambda(\omega'), \quad (36)$$

where the coefficient on the left-hand side is defined as

$$S_{\mu,\mu'}(\omega) \equiv [\hbar\omega_\mu - \hbar\omega - i\gamma_{\rm ex}/2]\delta_{\mu,\mu'} - \mu_0\omega^2\int d\boldsymbol{r}\int d\boldsymbol{r}'\ \boldsymbol{\mathcal{P}}_\mu^*(\boldsymbol{r})\cdot\overleftrightarrow{\mathsf{G}}(\boldsymbol{r},\boldsymbol{r}',\omega)\cdot\boldsymbol{\mathcal{P}}_{\mu'}(\boldsymbol{r}'). \quad (37)$$

The last term of Eq. (37) represents the self-energy due to the retarded interaction through the electromagnetic fields and

to the longitudinal Coulomb interaction. Further, Eq. (21) for $\check{b}^{(1)}_{\mu}(\omega)$ in the linear regime is also rewritten as

$$\sum_{\mu'} S_{\mu,\mu'}(\omega)\check{b}^{(1)}_{\mu'}(\omega) = \int d\boldsymbol{r}\ \boldsymbol{\mathcal{P}}^{*}_{\mu}(\boldsymbol{r})\cdot\check{\boldsymbol{E}}^{+}_{0}(\boldsymbol{r},\omega) + \check{\mathcal{D}}_{\mu}(\omega). \tag{38}$$

This simultaneous linear equation set is solved by calculating the inverse matrix $\overleftrightarrow{\mathsf{W}}(\omega) = [\overleftrightarrow{\mathsf{S}}(\omega)]^{-1}$, and the commutation relation of $\check{b}^{(1)}_{\mu}(\omega)$ is derived in Ref. 44 as

$$\left[\check{b}^{(1)}_{\mu}(\omega),\{\check{b}^{(1)}_{\mu'}(\omega'^{*})\}^{\dagger}\right] = \delta(\omega-\omega')\frac{\hbar}{i2\pi}[W_{\mu,\mu'}(\omega) - W^{*}_{\mu',\mu}(\omega)], \tag{39a}$$

$$\left[\check{b}^{(1)}_{\mu}(\omega),\check{b}^{(1)}_{\mu'}(-\omega')\right] = 0. \tag{39b}$$

Further, Eq. (36) is rewritten as

$$\check{b}_{\mu}(\omega) \simeq \check{b}^{(1)}_{\mu}(\omega) + \sum_{\mu',\lambda,\nu} W_{\mu,\mu'}(\omega)(\hbar\omega_{\mu'} + \hbar\omega_{\nu} - \hbar\Omega_{\lambda}) \times F_{\lambda,\mu',\nu}\int_{-\infty}^{\infty} d\omega'\left\{\check{b}^{(1)}_{\nu}(\omega'-\omega)\right\}^{\dagger}\mathcal{B}_{\lambda}(\omega'), \tag{40}$$

and, by substituting this into Eq. (33), the electric field involving RHPS is expressed under the RWA and the approximations discussed in Sec. II C as

$$\check{\boldsymbol{E}}^{+}(\boldsymbol{r},\omega) \simeq \check{\boldsymbol{E}}^{+}_{0}(\boldsymbol{r},\omega) + \sum_{\mu}\boldsymbol{\mathcal{E}}_{\mu}(\boldsymbol{r},\omega)\check{b}^{(1)}_{\mu}(\omega) + \check{\boldsymbol{E}}_{\mathrm{NL}}(\boldsymbol{r},\omega), \tag{41}$$

where

$$\boldsymbol{\mathcal{E}}_{\mu}(\boldsymbol{r},\omega) \equiv \mu_0\omega^2\int d\boldsymbol{r}'\ \overleftrightarrow{\mathsf{G}}(\boldsymbol{r},\boldsymbol{r}',\omega)\cdot\boldsymbol{\mathcal{P}}_{\mu}(\boldsymbol{r}'), \tag{42}$$

$$\check{\boldsymbol{E}}^{+}_{\mathrm{NL}}(\boldsymbol{r},\omega) = \sum_{\mu,\mu',\lambda,\nu}\boldsymbol{\mathcal{E}}_{\mu}(\boldsymbol{r},\omega)W_{\mu,\mu'}(\omega)(\hbar\omega_{\mu'} + \hbar\omega_{\nu} - \hbar\Omega_{\lambda}) \times F_{\lambda,\mu',\nu}\int_{-\infty}^{\infty} d\omega'\left\{\check{b}^{(1)}_{\nu}(\omega'-\omega)\right\}^{\dagger}\mathcal{B}_{\lambda}(\omega'). \tag{43}$$

F. Input and output fields

Here, we must pay attention to the electric field $\check{\boldsymbol{E}}^{+}_{0}(\boldsymbol{r},\omega)$ in the background system, which represents not only the field from matter to an observing point $\boldsymbol{r}$ but also the field from $\boldsymbol{r}$ to the matter. This means that the latter contribution must be removed from Eq. (41) to calculate observables, while the other terms involving $\check{b}^{(1)}_{\mu}(\omega)$ and $\check{\boldsymbol{E}}_{\mathrm{NL}}(\boldsymbol{r},\omega)$ represent the contribution emitted from the matter. While such a calculation has been usually treated by the input-output relations,[41,59–63] we use the following treatment based on the dyadic Green's function $\overleftrightarrow{\mathsf{G}}(\boldsymbol{r},\boldsymbol{r}',\omega)$ for $\check{\boldsymbol{E}}^{+}_{0}(\boldsymbol{r},\omega)$.

We separate $\check{\boldsymbol{E}}^{+}_{0}(\boldsymbol{r},\omega)$ into an input field $\check{\boldsymbol{E}}^{+}_{0,\mathrm{IN}}(\boldsymbol{r},\omega)$ from $\boldsymbol{r}$ to the matter and an output field $\check{\boldsymbol{E}}^{+}_{0,\mathrm{OUT}}(\boldsymbol{r},\omega)$ from the matter to $\boldsymbol{r}$ as

$$\check{\boldsymbol{E}}^{+}_{0}(\boldsymbol{r},\omega) = \check{\boldsymbol{E}}^{+}_{0,\mathrm{IN}}(\boldsymbol{r},\omega) + \check{\boldsymbol{E}}^{+}_{0,\mathrm{OUT}}(\boldsymbol{r},\omega). \tag{44}$$

By considering the causality, the output field at time t should be correlated only with fields at $t' < t$, and the commutation relation should be written as

$$[\check{\boldsymbol{E}}^{+}_{0,\mathrm{OUT}}(\boldsymbol{r},\omega),\check{\boldsymbol{E}}^{-}_{0}(\boldsymbol{r}',\omega')] = \frac{1}{(2\pi)^2}\int_{-\infty}^{\infty}dt'\int_{t'}^{\infty}dt\ e^{i\omega t - i\omega' t'}[\hat{\boldsymbol{E}}_0(\boldsymbol{r},t),\hat{\boldsymbol{E}}_0(\boldsymbol{r}',t')] = \delta(\omega-\omega')\frac{\mu_0\hbar\omega^2}{i2\pi}\overleftrightarrow{\mathsf{G}}(\boldsymbol{r},\boldsymbol{r}',\omega), \tag{45}$$

where we use the fact that the dyadic Green's function $\overleftrightarrow{\mathsf{G}}(\boldsymbol{r},\boldsymbol{r}',\omega)$ satisfying Eq. (32) is the retarded correlation function of the electric field:[44,68]

$$-\mu_0\omega^2\overleftrightarrow{\mathsf{G}}(\boldsymbol{r},\boldsymbol{r}',\omega) = \frac{1}{i\hbar}\int_{t'}^{\infty}dt\ e^{i\omega(t-t')}\langle[\hat{\boldsymbol{E}}_0(\boldsymbol{r},t),\hat{\boldsymbol{E}}_0(\boldsymbol{r}',t')]\rangle. \tag{46}$$

In the same manner, the input field at t should be correlated only with fields at $t' > t$, and the commutation relation is derived as

$$[\check{\boldsymbol{E}}^{+}_{0,\mathrm{IN}}(\boldsymbol{r},\omega),\check{\boldsymbol{E}}^{-}_{0}(\boldsymbol{r}',\omega')] = \frac{1}{(2\pi)^2}\int_{-\infty}^{\infty}dt'\int_{-\infty}^{t'}dt\ e^{i\omega t - i\omega' t'}[\hat{\boldsymbol{E}}_0(\boldsymbol{r},t),\hat{\boldsymbol{E}}_0(\boldsymbol{r}',t')] = -\delta(\omega-\omega')\frac{\mu_0\hbar\omega^2}{i2\pi}\overleftrightarrow{\mathsf{G}}^{*}(\boldsymbol{r},\boldsymbol{r}',\omega). \tag{47}$$

Actually, Eqs. (45) and (47) reproduce Eq. (35). By using the output field $\check{\boldsymbol{E}}^{+}_{0,\mathrm{OUT}}(\boldsymbol{r},\omega)$ in the background system, we define the scattering field excluding the input one as

$$\check{\boldsymbol{E}}^{+}_{\mathrm{RHPS}}(\boldsymbol{r},\omega) \equiv \check{\boldsymbol{E}}^{+}(\boldsymbol{r},\omega) - \check{\boldsymbol{E}}^{+}_{0,\mathrm{IN}}(\boldsymbol{r},\omega) = \check{\boldsymbol{E}}^{+}_{\mathrm{LIN}}(\boldsymbol{r},\omega) + \check{\boldsymbol{E}}^{+}_{\mathrm{NL}}(\boldsymbol{r},\omega), \tag{48}$$

where $\check{\boldsymbol{E}}^{+}_{\mathrm{LIN}}(\boldsymbol{r},\omega)$ is the linear component of the electric field excluding the input field as

$$\check{\boldsymbol{E}}^{+}_{\mathrm{LIN}}(\boldsymbol{r},\omega) = \check{\boldsymbol{E}}^{+}_{0,\mathrm{OUT}}(\boldsymbol{r},\omega) + \sum_{\mu}\boldsymbol{\mathcal{E}}_{\mu}(\boldsymbol{r},\omega)\check{b}^{(1)}_{\mu}(\omega). \tag{49}$$

By deriving commutation relations of $\check{\boldsymbol{E}}_{\mathrm{LIN}}(\boldsymbol{r},\omega)$ and $\check{\boldsymbol{E}}_{\mathrm{NL}}(\boldsymbol{r},\omega)$ from Eqs. (35), (39), and (45), we can evaluate the observables of RHPS.

III. PRACTICAL CALCULATION

Next, we apply the theoretical framework discussed in the previous section into multilayer systems embedding a CuCl layer, and derive expressions of one-photon scattering intensity and two-photon coincidence intensity by RHPS. An incident light beam propagates along the z axis (perpendicular to the surface), and photon pairs emitted into the x-z plane are considered (in-plane wave vector is in x direction). We suppose that center-of-mass motions of excitons and biexcitons are confined in the CuCl layer with thickness d existing at $0 < z < d$. Since we consider a large enough thickness d compared to the Bohr radii of exciton (0.7 nm) and of biexciton (1.5 nm),[65] the relative motions of excitons and biexcitons are not strongly modified from the ones in bulk crystals, and all the information of the relative motion is described by factors

M and Φ in Eqs. (8) and (30). As seen in Fig. 2(a), the center-of-mass wave functions of excitons and biexcitons are expanded by a series of sinusoidal functions as

$$g^{\rm bx}_{\bar{k},m}(\boldsymbol{r}) = g^{\rm ex}_{\bar{k},m}(\boldsymbol{r}) = \theta(z)\frac{e^{i\bar{k}x}}{\sqrt{S}}\sqrt{\frac{2}{d}}\sin(q_m z), \tag{50}$$

where $\theta(z)$ gives unity for $0 < z < d$ and zero otherwise, $\bar{k}$ is the in-plane wave number, S is the normalization area in the $x-y$ plane, and $q_m = m\pi/d$ is the confinement wave number in the z direction for $m = 1, 2, \ldots$. We consider $\varepsilon_{\rm bg}(\boldsymbol{r},\omega)$ as a discontinuous steplike function in the z direction representing the background dielectric constant in each layer, and it does not depend on ω nor $\boldsymbol{r}_\parallel$. In the case of the multilayer structure in Fig. 2(b), $\varepsilon_{\rm bg}(\boldsymbol{r},\omega)$ gives the background dielectric constant $\varepsilon^{\rm ex}_{\rm bg}$ for excitons at the CuCl layer; otherwise it gives the dielectric constant of each layer. According to Ref. 67, if z' is in the CuCl layer, the dyadic Green's function satisfying Eq. (32) is expressed as

$$\begin{aligned}\overleftrightarrow{\mathsf{G}}_{\bar{k}}(z,z',\omega) &\equiv \int d\boldsymbol{r}_\parallel \int d\boldsymbol{r}'_\parallel \frac{e^{-i\bar{k}(x-x')}}{S}\overleftrightarrow{\mathsf{G}}(\boldsymbol{r},\boldsymbol{r}',\omega)\\ &= -\frac{1}{i2k^{\rm ex}_{\rm bg}}\left[\overleftrightarrow{\mathcal{G}}^{V}_{\bar{k}}(z,z',\omega) + \overleftrightarrow{\mathcal{G}}^{H}_{\bar{k}}(z,z',\omega)\right]\\ &\quad - \frac{\boldsymbol{e}_z\boldsymbol{e}_z}{\varepsilon^{\rm ex}_{\rm bg}\omega^2/c^2}\delta(z-z'),\end{aligned} \tag{51}$$

where $k^{\rm ex2}_{\rm bg} = \varepsilon^{\rm ex}_{\rm bg}\omega^2/c^2 - \bar{k}^2$, and $\boldsymbol{e}_\xi$ is the unit vector in ξ direction. When z is in layer j with dielectric constant ε_j, the tensors in Eq. (51) are written as

$$\overleftrightarrow{\mathcal{G}}^{V}_{\bar{k}}(z,z',\omega) = \boldsymbol{e}_y\boldsymbol{e}_y\mathcal{G}^{V}_{\bar{k}}(z,z',\omega), \tag{52}$$

$$\overleftrightarrow{\mathcal{G}}^{H}_{\bar{k}}(z,z',\omega) = \begin{pmatrix} \mathrm{D}_z\mathrm{D}'_z & 0 & i\mathrm{D}_z\bar{k} \\ 0 & 0 & 0 \\ -i\bar{k}\mathrm{D}'_z & 0 & \bar{k}^2 \end{pmatrix}\frac{\mathcal{G}^{H}_{\bar{k}}(z,z',\omega)}{\sqrt{\varepsilon^{\rm ex}_{\rm bg}\varepsilon_j}\omega^2/c^2}, \tag{53}$$

where $\mathrm{D}_z \equiv \partial/\partial z$ and $\mathrm{D}'_z \equiv \partial/\partial z'$. Equations (52) and (53), respectively, describe the propagation of V- and H-polarized fields, and, according to Ref. 67, $\mathcal{G}^{V/H}_{\bar{k}}(z,z')$ is expressed as follows.

When z is in the CuCl layer ($0 < z < d$),

$$\begin{aligned}&\mathcal{G}^{V/H}_{\bar{k}}(z,z')\\ &= \mathrm{e}^{ik^{\rm ex}_{\rm bg}|z-z'|} + e^{ik^{\rm ex}_{\rm bg}z}\tilde{R}^{V/H}_{L}\left[e^{ik^{\rm ex}_{\rm bg}z'} + \tilde{R}^{V/H}_{R}e^{ik^{\rm ex}_{\rm bg}(2d-z')}\right]\tilde{M}^{V/H}\\ &\quad + \mathrm{e}^{-ik^{\rm ex}_{\rm bg}(z-d)}\tilde{R}^{V/H}_{R}\left[e^{ik^{\rm ex}_{\rm bg}(d-z')} + \tilde{R}^{V/H}_{L}e^{ik^{\rm ex}_{\rm bg}(d+z')}\right]\tilde{M}^{V/H}.\end{aligned} \tag{54a}$$

When z is in the leftmost semi-infinite region,

$$\mathcal{G}^{V/H}_{\bar{k}}(z,z') = \mathrm{e}^{-ik_L z}\tilde{T}^{V/H}_{L}\left[\mathrm{e}^{ik^{\rm ex}_{\rm bg}z'} + \tilde{R}^{V/H}_{R}\mathrm{e}^{ik^{\rm ex}_{\rm bg}(2d-z')}\right]\tilde{M}^{V/H}. \tag{54b}$$

When z is in the rightmost semi-infinite region,

$$\mathcal{G}^{V/H}_{\bar{k}}(z,z') = \mathrm{e}^{ik_R z}\tilde{T}^{V/H}_{R}\left[\mathrm{e}^{ik^{\rm ex}_{\rm bg}(d-z')} + \tilde{R}^{V/H}_{L}\mathrm{e}^{ik^{\rm ex}_{\rm bg}(d+z')}\right]\tilde{M}^{V/H}. \tag{54c}$$

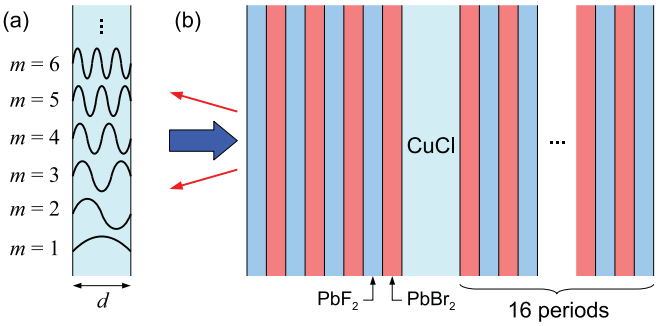

FIG. 2. (Color online) (a) Center-of-mass wave functions of excitons and biexcitons in a CuCl film. Simple sinusoidal functions vanishing at surfaces are supposed. (b) Cavity structure considered in Figs. 9 and 10. The Bragg mirrors consist of $PbBr_2$ and PbF_2. On the transmission side, a high reflectance is achieved by a mirror with 16 periods to suppress the leakage of photons in this direction. On the incident side, only 4 periods are supposed to guarantee rapid radiative decay of entangled photons.

Here, $\tilde{R}^{V/H}_{L(R)}$ represents the generalized reflection coefficient for the V/H-polarized field from the CuCl layer against the left(right)-hand neighboring, and $\tilde{T}^{V/H}_{L(R)}$ is the generalized transmission coefficient from the CuCl layer to the left(right) most region. The derivation of these coefficients is shown in Ref. 67. Further, ${k_{L(R)}}^2 = \varepsilon_{L(R)}\omega^2/c^2 - \bar{k}^2$ is the wave number in the left(right)most region with dielectric constant $\varepsilon_{L(R)}$, and the factor $\tilde{M}^{V/H}$ is defined as $\tilde{M}^{V/H} = [1 - \tilde{R}^{V/H}_{L}\tilde{R}^{V/H}_{R}e^{i2k^{\rm ex}_{\rm bg}d}]^{-1}$.

From Eqs. (50) and (51), we can evaluate the coefficient matrix $\overleftrightarrow{\mathsf{S}}(\omega)$ [Eq. (37)] and numerically calculate the inverse matrix $\overleftrightarrow{\mathsf{W}}(\omega) = [\overleftrightarrow{\mathsf{S}}(\omega)]^{-1}$. From Eq. (38), the amplitude of excitons is obtained in the linear regime by

$$\left\langle \check{b}^{(1)}_{\mu}(\omega)\right\rangle = \sum_{\mu'} W_{\mu,\mu'}(\omega)\int d\boldsymbol{r}\,\boldsymbol{\mathcal{P}}^{*}_{\mu'}(\boldsymbol{r})\cdot\langle\check{\boldsymbol{E}}^{+}_{0}(\boldsymbol{r},\omega)\rangle. \tag{55}$$

Here, $\langle\check{\boldsymbol{E}}^{+}_{0}(\boldsymbol{r},\omega)\rangle$ represents the pump field, i.e., the amplitude of electric field in the background dielectric system $\hat{H}_{\rm em}$, and can be derived by the standard transfer matrix method[67] in the case of dielectric multilayers. For simplicity, we consider a monochromatic laser light with frequency $\omega_{\rm in}$ with in-plane wave number $\bar{k}_{\rm in}$. Concerning the pump power $I_{\rm in}$ ($\langle\check{\boldsymbol{E}}^{+}_{0}\rangle \propto \sqrt{I_{\rm in}}$), there is a scaling law for the intensity of entangled photons as explained below. In the present paper, since we only consider the $1s$ exciton and the lowest biexciton level, the exciton states are labeled by polarization direction $\xi = \{x,y,z\}$, in-plane wave number $\bar{k}$, and index m of center-of-mass motion as $\mu = \{\xi,\bar{k},m\}$, and the biexciton states are labeled by $\lambda = \{\bar{k},m\}$. Considering the conservations of energy and in-plane wave vector, the amplitude of biexciton is evaluated by Eq. (23), and we denote it as

$$\mathcal{B}_{\bar{k},m}(\omega) = \delta_{\bar{k},2\bar{k}_{\rm in}}\delta(\omega - 2\omega_{\rm in})\tilde{\mathcal{B}}_{2\bar{k}_{\rm in},m}(2\omega_{\rm in}). \tag{56}$$

Further, the linear and nonlinear components of the scattering field [Eqs. (49) and (43)] are simply rewritten as

$$\begin{aligned}\check{\boldsymbol{E}}^{+}_{\mathrm{LIN},\bar{k}}(z,\omega) &= \frac{1}{\sqrt{S}}\int d\boldsymbol{r}_{\parallel}\, e^{-i\bar{k}x}\check{\boldsymbol{E}}^{+}_{\mathrm{LIN}}(\boldsymbol{r},\omega)\\ &= \check{\boldsymbol{E}}^{+}_{0,\mathrm{OUT},\bar{k}}(z,\omega)+\sum_{\xi,m}\boldsymbol{\mathcal{E}}_{\xi,\bar{k},m}(z,\omega)\check{b}^{(1)}_{\xi,\bar{k},m}(\omega),\end{aligned} \tag{57}$$

$$\begin{aligned}\check{\boldsymbol{E}}^{+}_{\mathrm{NL},\bar{k}}(z,\omega) &= \frac{1}{\sqrt{S}}\int d\boldsymbol{r}_{\parallel}\, e^{-i\bar{k}x}\check{\boldsymbol{E}}^{+}_{\mathrm{NL}}(\boldsymbol{r},\omega)\\ &= \sum_{\xi,m}\boldsymbol{\mathcal{E}}^{\mathrm{NL}}_{\xi,\bar{k}_{\mathrm{in}},\bar{k},m}(z,\omega_{\mathrm{in}},\omega)\{\check{b}^{(1)}_{\xi,2\bar{k}_{\mathrm{in}}-\bar{k},m}(2\omega_{\mathrm{in}}-\omega)\}^{\dagger},\end{aligned} \tag{58}$$

where the coefficients are evaluated by the following quantities and functions:

$$\boldsymbol{\mathcal{E}}_{\xi,\bar{k},m}(z,\omega) = \mu_0\omega^2 M\sqrt{\frac{1}{d}}\int dz'\ \overleftrightarrow{\mathsf{G}}_{\bar{k}}(z,z',\omega)\cdot\boldsymbol{e}_{\xi}\sin(q_m z')\theta(z'), \tag{59}$$

$$\begin{aligned}\boldsymbol{\mathcal{E}}^{\mathrm{NL}}_{\xi,\bar{k}_{\mathrm{in}},\bar{k},m}(z,\omega_{\mathrm{in}},\omega) = &\sum_{\xi',\xi'',m',m'',n}\boldsymbol{\mathcal{E}}_{\xi'',\bar{k},m''}(z,\omega)W_{\{\xi'',\bar{k},m''\},\{\xi',\bar{k},m'\}}(\omega)(\hbar\omega_{\xi',\bar{k},m'}\\ &+\hbar\omega_{\xi,2\bar{k}_{\mathrm{in}}-\bar{k},m}-\hbar\Omega_{2\bar{k}_{\mathrm{in}},n})F_{\{2\bar{k}_{\mathrm{in}},n\},\{\xi',\bar{k},m'\},\{\xi,2\bar{k}_{\mathrm{in}}-\bar{k},m\}}\tilde{\mathcal{B}}_{2\bar{k}_{\mathrm{in}},n}(2\omega_{\mathrm{in}}),\end{aligned} \tag{60}$$

$$F_{\{2\bar{k}_{\mathrm{in}},n\},\{\xi',\bar{k},m'\},\{\xi,\bar{k}',m\}} = \delta_{\xi,\xi'}\delta_{\bar{k}',2\bar{k}_{\mathrm{in}}-\bar{k}}\Phi\left(\frac{2}{d}\right)^{3/2}\int dz\,\theta(z)\sin(q_n z)\sin(q_m z)\sin(q_{m'}z), \tag{61}$$

$$\begin{aligned}S_{\{\xi,\bar{k},m\},\{\xi',\bar{k}',m'\}}(\omega) = &[\hbar\omega_{\xi,\bar{k},m}-\hbar\omega-i\gamma_{\mathrm{ex}}/2]\delta_{\xi,\xi'}\delta_{\bar{k},\bar{k}'}\delta_{m,m'}\\ &-\delta_{\bar{k},\bar{k}'}\mu_0\omega^2|M|^2\int dz\int dz'\,\theta(z)\theta(z')\boldsymbol{e}_{\xi}\cdot\overleftrightarrow{\mathsf{G}}_{\bar{k}}(z,z',\omega)\cdot\boldsymbol{e}_{\xi'}\sin(q_m z)\sin(q_{m'}z').\end{aligned} \tag{62}$$

Further, from the commutation relations (39) and (45), the following relations are derived for $\omega > 0$ and $\omega' > 0$ as

$$\begin{aligned}&[\check{\boldsymbol{E}}^{+}_{\mathrm{LIN},\bar{k}}(z,\omega),\check{\boldsymbol{E}}^{+}_{\mathrm{NL},\bar{k}'}(z,\omega')]\\ &\quad=\delta_{\bar{k}',2\bar{k}_{\mathrm{in}}-\bar{k}}\delta(\omega+\omega'-2\omega_{\mathrm{in}})\overleftrightarrow{\mathsf{H}}^{\mathrm{LN}}_{\bar{k}_{\mathrm{in}},\bar{k}}(z,z',\omega_{\mathrm{in}},\omega),\end{aligned} \tag{63a}$$

$$[\check{\boldsymbol{E}}^{+}_{\mathrm{LIN},\bar{k}}(z,\omega),\check{\boldsymbol{E}}^{-}_{\mathrm{NL},\bar{k}'}(z',\omega')] = \overleftrightarrow{\mathbf{0}}, \tag{63b}$$

$$\begin{aligned}&[\check{\boldsymbol{E}}^{-}_{\mathrm{NL},\bar{k}}(z,\omega),\check{\boldsymbol{E}}^{+}_{\mathrm{NL},\bar{k}'}(z',\omega')]\\ &\quad=\delta_{\bar{k},\bar{k}'}\delta(\omega-\omega')\overleftrightarrow{\mathsf{H}}^{\mathrm{NN}}_{\bar{k}_{\mathrm{in}},\bar{k}}(z,z',\omega_{\mathrm{in}},\omega),\end{aligned} \tag{64a}$$

$$[\check{\boldsymbol{E}}^{+}_{\mathrm{NL},\bar{k}}(z,\omega),\check{\boldsymbol{E}}^{+}_{\mathrm{NL},\bar{k}'}(z',\omega')] = \overleftrightarrow{\mathbf{0}}, \tag{64b}$$

where the tensors are defined as

$$\begin{aligned}\overleftrightarrow{\mathsf{H}}^{\mathrm{LN}}_{\bar{k}_{\mathrm{in}},\bar{k}}(z,z',\omega_{\mathrm{in}},\omega) \equiv &\frac{\hbar}{i2\pi}\sum_{\xi,\xi',m,m'}\boldsymbol{\mathcal{E}}_{\xi,\bar{k},m}(z,\omega)\\ &\times W_{\{\xi,\bar{k},m\},\{\xi',\bar{k},m'\}}(\omega)\boldsymbol{\mathcal{E}}^{\mathrm{NL}}_{\xi',\bar{k}_{\mathrm{in}},2\bar{k}_{\mathrm{in}}-\bar{k},m'}\\ &\times(z',\omega_{\mathrm{in}},2\omega_{\mathrm{in}}-\omega),\end{aligned} \tag{65}$$

$$\begin{aligned}\overleftrightarrow{\mathsf{H}}^{\mathrm{NN}}_{\bar{k}_{\mathrm{in}},\bar{k}}(z,z',\omega_{\mathrm{in}},\omega) \equiv &\frac{\hbar}{i2\pi}\sum_{\xi,\xi',m,m'}\boldsymbol{\mathcal{E}}^{\mathrm{NL}*}_{\xi,\bar{k}_{\mathrm{in}},\bar{k},m}(z,\omega)\\ &\times[W_{\{\xi,2\bar{k}_{\mathrm{in}}-\bar{k},m\},\{\xi',2\bar{k}_{\mathrm{in}}-\bar{k},m'\}}(2\omega_{\mathrm{in}}-\omega)\\ &-W^{*}_{\{\xi',2\bar{k}_{\mathrm{in}}-\bar{k},m'\},\{\xi,2\bar{k}_{\mathrm{in}}-\bar{k},m\}}(2\omega_{\mathrm{in}}-\omega)]\\ &\times\boldsymbol{\mathcal{E}}^{\mathrm{NL}}_{\xi',\bar{k}_{\mathrm{in}},\bar{k},m'}(z',\omega_{\mathrm{in}},\omega).\end{aligned} \tag{66}$$

From these commutation relations, we calculate the one-photon scattering intensity and the two-photon coincidence intensity. When the background field $\check{\boldsymbol{E}}_{0,\bar{k}}(z)$ is the vacuum state in the scattering direction determined by $\bar{k}$ and only has the quantum fluctuation, we obtain the following relations for the initial condition $|0\rangle$, which is not affected by the exciton-exciton scattering:

$$\begin{aligned}\check{\boldsymbol{E}}^{+}_{0,\bar{k}}(z,\omega)|0\rangle &= \check{\boldsymbol{E}}^{+}_{0,\mathrm{OUT},\bar{k}}(z,\omega)|0\rangle = \check{\boldsymbol{E}}^{+}_{\mathrm{LIN},\bar{k}}(z,\omega)|0\rangle\\ &= \check{\boldsymbol{E}}^{-}_{\mathrm{NL},\bar{k}}(z,\omega)|0\rangle = \mathbf{0}.\end{aligned} \tag{67}$$

When we measure the one-photon scattering intensity in the direction $\bar{k}$ at position z with polarization direction ξ and frequency ω by resolution $\Delta\omega$, the intensity is represented as

$$\begin{aligned}C^{(1)}_{\xi,\bar{k}_{\mathrm{in}},\bar{k}}(z,\omega_{\mathrm{in}},\omega) &= \int_{\omega-\Delta\omega/2}^{\omega+\Delta\omega/2}d\omega' d\omega''\\ &\quad\times\langle\check{E}^{-}_{\mathrm{RHPS},\bar{k},\xi}(z,\omega')\check{E}^{+}_{\mathrm{RHPS},\bar{k},\xi}(z,\omega'')\rangle\\ &= \Delta\omega\left[\overleftrightarrow{\mathsf{H}}^{\mathrm{NN}}_{\bar{k}_{\mathrm{in}},\bar{k}}(z,z,\omega_{\mathrm{in}},\omega)\right]_{\xi,\xi},\end{aligned} \tag{68}$$

where $\check{E}^{\pm}_{\mathrm{RHPS},\bar{k},\xi}$ is the ξ component of $\check{\boldsymbol{E}}^{\pm}_{\mathrm{RHPS},\bar{k}}$ and $[\cdots]_{\xi,\xi'}$ extracts the (ξ,ξ') component of the tensor. Here, it is worth noting that this one-photon scattering intensity is proportional to $I_{\mathrm{in}}{}^2$, the square of the pump power, reflecting the power dependence of the biexciton creation. The z dependence of this function only represents the scattering direction to the left- or right-hand side, if the leftmost and rightmost regions are nonabsorptive. On the other hand, when we measure

the two-photon coincidence between the scattering fields of $(\xi_1,\bar{k}_1,z_1,\omega_1)$ and $(\xi_2,\bar{k}_2,z_2,\omega_2)$, the intensity is represented as

$$\begin{aligned} &C^{(2)}_{\xi_1,\xi_2,\bar{k}_{\rm in},\bar{k}_1,\bar{k}_2}(z_1,z_2,\omega_{\rm in},\omega_1,\omega_2) \\ &= \int_{\omega_1-\Delta\omega/2}^{\omega_1+\Delta\omega/2} d\omega_1' d\omega_1'' \int_{\omega_2-\Delta\omega/2}^{\omega_2+\Delta\omega/2} d\omega_2' d\omega_2'' \\ &\times \langle \check{E}^-_{{\rm RHPS},\bar{k}_1,\xi_1}(z_1,\omega_1') \check{E}^-_{{\rm RHPS},\bar{k}_2,\xi_2}(z_2,\omega_2') \\ &\times \check{E}^+_{{\rm RHPS},\bar{k}_2,\xi_2}(z_2,\omega_2'') \check{E}^+_{{\rm RHPS},\bar{k}_1,\xi_1}(z_1,\omega_1'')\rangle. \end{aligned} \tag{69}$$

By using the above commutation relations, we finally get

$$\begin{aligned} &C^{(2)}_{\xi_1,\xi_2,\bar{k}_{\rm in},\bar{k}_1,\bar{k}_2}(z_1,z_2,\omega_{\rm in},\omega_1,\omega_2) \\ &= \delta_{\bar{k}_2,2\bar{k}_{\rm in}-\bar{k}_1}\tilde{\delta}(\omega_1+\omega_2,2\omega_{\rm in}) C^{(2){\rm S}}_{\xi_1,\xi_2,\bar{k}_{\rm in},\bar{k}_1}(z_1,z_2,\omega_{\rm in},\omega_1) \\ &+ C^{(2){\rm N}}_{\xi_1,\xi_2,\bar{k}_{\rm in},\bar{k}_1,\bar{k}_2}(z_1,z_2,\omega_{\rm in},\omega_1,\omega_2) \\ &+ (\Delta\omega)^2 \delta_{\bar{k}_1,\bar{k}_2}\tilde{\delta}(\omega_1,\omega_2) \left[\overleftrightarrow{\rm H}^{\rm NN}_{\bar{k}_{\rm in},\bar{k}_1}(z_1,z_2,\omega_1)\right]_{\xi_1,\xi_2} \\ &\times \left[\overleftrightarrow{\rm H}^{\rm NN}_{\bar{k}_{\rm in},\bar{k}_2}(z_2,z_1,\omega_2)\right]_{\xi_2,\xi_1}. \end{aligned} \tag{70}$$

Here, the function $\tilde{\delta}(\omega,\omega')$ gives unity for $\omega \simeq \omega'$ and zero otherwise. The first term represents the signal intensity, i.e., the number of correlated photon pairs, which satisfies the energy conservation $\omega_1+\omega_2 \simeq 2\omega_{\rm in}$ by resolution $\Delta\omega$, and the signal intensity is calculated as

$$\begin{aligned} &C^{(2){\rm S}}_{\xi_1,\xi_2,\bar{k}_{\rm in},\bar{k}_1}(z_1,z_2,\omega_{\rm in},\omega_1) \\ &\equiv (\Delta\omega)^2 \left| \left[\overleftrightarrow{\rm H}^{\rm LN}_{\bar{k}_{\rm in},2\bar{k}_{\rm in}-\bar{k}_1}(z_2,z_1,\omega_{\rm in},2\omega_{\rm in}-\omega_1)\right]_{\xi_2,\xi_1}\right|^2. \end{aligned} \tag{71}$$

This expression is invariant by exchanging the two observing conditions, and it is also proportional to ${I_{\rm in}}^2$, because one entangled-photon pair is emitted from one biexciton. On the other hand, the second term in Eq. (70) is nonzero for arbitrary pair ω_1 and ω_2, and represents the accidental coincidence of emitted photons from independent biexcitons, and it is represented as the product of two one-photon scattering intensities as

$$\begin{aligned} &C^{(2){\rm N}}_{\xi_1,\xi_2,\bar{k}_{\rm in},\bar{k}_1,\bar{k}_2}(z_1,z_2,\omega_{\rm in},\omega_1,\omega_2) \\ &\equiv C^{(1)}_{\xi_1,\bar{k}_{\rm in},\bar{k}_1}(z_1,\omega_{\rm in},\omega_1) C^{(1)}_{\xi_2,\bar{k}_{\rm in},\bar{k}_2}(z_2,\omega_{\rm in},\omega_2). \end{aligned} \tag{72}$$

This is also invariant by exchanging the two observing conditions, and proportional to ${I_{\rm in}}^4$. The third term in Eq. (70) represents the interference between the two observing points and is nonzero only for $\omega_1 \simeq \omega_2$. Therefore, we neglect this term in the following discussion.

According to Sec. 3.10 in Ref. 11, we suppose the translational masses of excitons and biexcitons as $m_{\rm ex} = 2.3m_0$ and $m_{\rm bx} = 2.3m_{\rm ex}$, respectively, where m_0 is the free-electron mass. These masses were measured by RHPS experiments.[11,50,51] However, in our calculation, we do not consider the mass difference between transverse and longitudinal excitons. From Sec. 3.2 in Ref. 11, the transverse exciton energy at band edge is $\hbar\omega_{\rm T} = 3.2022$eV, the LT splitting energy is $\Delta = 5.7$meV, and the background dielectric constant of CuCl is $\varepsilon^{ex}_{\rm bg} = 5.59$. Further, according to Sec. 3.7 in Ref. 11, the binding energy of the biexciton lowest level is $\Delta = 32.2$ meV. The energy of excitons including the center-of-mass kinetic energy is written as

$$\hbar\omega_{\xi,\bar{k},m} = \hbar\omega_{\rm T} + \frac{\hbar^2}{2m_{\rm ex}}(\bar{k}^2 + {q_m}^2). \tag{73}$$

The biexciton energy is

$$\hbar\Omega_{\bar{k},m} = 2\hbar\omega_{\rm T} - \Delta + \frac{\hbar^2}{2m_{\rm bx}}(\bar{k}^2 + {q_m}^2). \tag{74}$$

We use the other biexciton parameters reported in Ref. 53: The phenomenological damping width is $\gamma_{\rm bx} = \hbar/50\,{\rm ps} = 13.2\,\mu$eV, and the effective volume is $|\Phi|^2 = (4000/2) \times (0.541\ {\rm nm})^3/4 = 80\,{\rm nm}^3$, where 0.541 nm is the lattice constant of CuCl, and 4000 is a parameter representing the nonlinear strength. In most of all calculations, we consider the exciton nonradiative damping width as $\gamma_{\rm ex} = 0.5$ meV.

Because of the translational symmetry in the $x-y$ plane, the in-plane wave number in the system is conserved. In the following discussion, we suppose that the pump field is perpendicular to the layers, and biexcitons have zero in-plane wave number. Then, a scattered photon with $\bar{k}$ makes a pair with the one having $-\bar{k}$. However, their frequencies are different in general satisfying the energy conservation $\omega_1+\omega_2 = 2\omega_{\rm in}$. In the present paper, we define the scattering angle θ as $\bar{k} = (\omega_{\rm T}/c)\sin\theta$, which is approximately equal to the scattering angle in vacuum.

IV. RESULTS

By using the theoretical framework discussed in the previous sections, we calculate the scattering spectra by bulk crystal and by thin film in Sec. IV A. In Sec. IV B, we discuss the difference of entangled photon generation by thin film compared with the one by bulk crystal, and show the thickness dependence of generation efficiency and performance by RHPS. Finally, we discuss the generation from a DBR cavity embedding a CuCl layer in Sec. IV C.

A. Scattering spectra

Figure 3 shows forward (transmission side) scattering spectra of RHPS from a CuCl film with thickness $d = 7\mu$m. We plot $C^{(1)}_{\xi,\bar{k}_{\rm in}=0,\bar{k}=(\omega_{\rm T}/c)\sin\theta}(z>d,\omega_{\rm in},\omega)$ as a function of ω for scattering angles $\theta = 0^\circ$, 30°, and 60°, and the spectra are summed over the polarization direction $\xi = \{x,y,z\}$. The CuCl film exists in vacuum, and the pump frequency is tuned to the two-photon absorption involving biexcitons as $\hbar\omega_{\rm in} \simeq \hbar\omega_{\rm T} - \Delta/2$. Actually, $\hbar\omega_{\rm in}$ is not exactly $\hbar\omega_{\rm T} - \Delta/2$, because we must also consider the phase-matching condition (wave vector conservation) between two polariton branches and a biexciton one.[11] Since the shapes of scattering spectra do not depend on the input power $I_{\rm in}$, we plot the scattering intensity with arbitrary units. The decay paths of biexcitons are depicted in Fig. 1. As seen in Fig. 3, at $\theta = 0^\circ$, we can find multiple peaks at $\hbar\omega - \hbar\omega_{\rm T} \simeq -\Delta/2 = -16.1$ meV and a single peak at $\hbar\omega - \hbar\omega_{\rm T} \simeq -\Delta = 32.2$ meV. The latter is called the $M_{\rm T}$ peak, which is emitted by the biexciton relaxation into the transverse exciton level (exciton-like polariton).[11] The

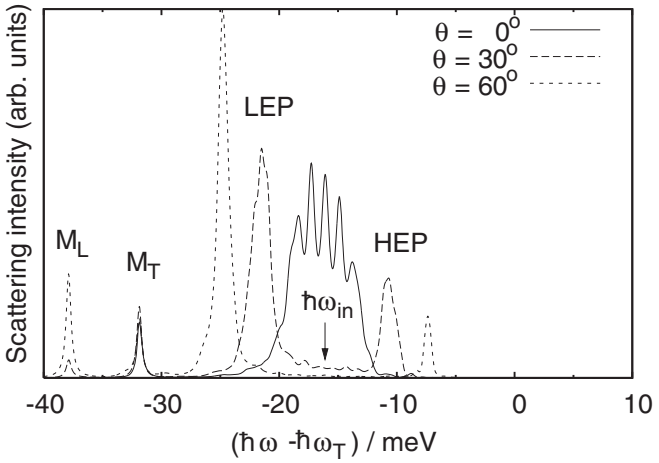

FIG. 3. Forward scattering spectra from a CuCl film with thickness $d = 7\mu$m. The film exists in vacuum, and the pump beam is perpendicular to it. The pump frequency $\omega_{\rm in}$ corresponds to the two-photon absorption involving biexcitons. The results for scattering angles $\theta = 0^\circ, 30^\circ$, and 60° are plotted with different lines as functions of scattering frequency ω.

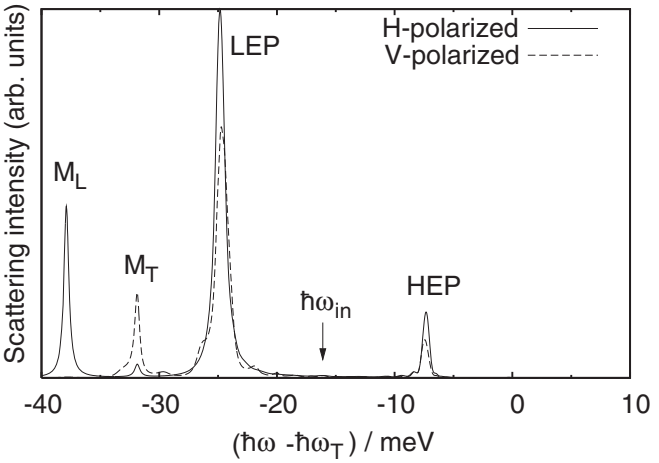

FIG. 4. The scattering spectra of horizontal (H) and vertical (V) polarizations are shown. The film thickness is $d = 7\mu$m, and the scattering angle is $\theta = 60^\circ$. The other parameters are the same as in Fig. 3.

remaining polariton with frequency $\omega \simeq \omega_{\rm T}$ propagates backward, but it cannot go outside the film because of the absorption. On the other hand, the multiple peaks at $\hbar\omega - \hbar\omega_{\rm T} \simeq -16.1$ meV originate from the biexciton relaxation into two polaritons, and the peak structure is due to the interference inside the film with $d = 7\mu$m. Increasing the scattering angle, the entangled peaks are split into lower and higher energy sides satisfying the energy and wave vector conservations as discussed in Ref. 37. These peaks are the LEP and HEP, and the intensity of HEP is usually smaller than that of LEP, because of the strong absorption near the bare exciton energy $\omega_{\rm T}$. The angle dependence of the peak positions obeys the relation shown in Ref. 37. The peak at $\hbar\omega - \hbar\omega_{\rm T} \simeq -\Delta_{\rm bx} - \Delta_{\rm LT}$ is called $\rm M_L$, which is emitted by the biexciton relaxation into the longitudinal exciton state. The emitted photon cannot go outside when $\theta = 0^\circ$ because it is polarized in the z direction (longitudinal), and the remaining exciton also cannot go outside due to the strong absorption even for $\theta > 0^\circ$.

Figure 4 shows the polarization-resolved scattering spectra. The film thickness is also $d = 7\mu$m and the scattering angle is $\theta = 60^\circ$. H and V represent the horizontal and vertical polarizations, respectively, with respect to the scattering plane. The $\rm M_L$ peak consists of only H-polarized light, because V-polarization does not contain the longitudinal component. Concerning the LEP and HEP peaks, their intensities depend on the polarization direction. This is a general aspect at nonzero scattering angles, because the reflectance at the surface is in general different for the two polarizations. When we resolve the spectra with circular polarizations, the spectra of left- and right-polarizations are the same for any scattering angles and any frequencies.

Figure 5(a) shows the polarization-resolved scattering spectra at thickness $d = 200$ nm. The scattering angle is $\theta = 60^\circ$ and the pump frequency is tuned to excite the $m = 6$ biexciton state. Compared with the spectra by bulk crystal in Fig. 4, there are more than two peaks in the LEP-HEP frequency region. The peak positions are different for H and V polarizations, and they do not obey the angle-frequency relation for bulk crystal.[37] The spectral shape can be interpreted by the exciton-photon coupled modes[17,18,21,32,33,35] in the thin film, which have been discussed in relation with the radiative decay of excitons in the nano-to-bulk crossover regime.[22–25] Due to the breaking of translational symmetry in the z direction, the lower and upper polaritons in bulk material are no longer good eigenstates. Instead, we obtain the exciton-photon coupled modes with discrete energy levels and radiative decay rates in the case of thin film. A created biexciton spontaneously decays into these coupled modes with emitting a photon conserving the energy and in-plane wave vector. By using the method in Ref. 18, we calculated the exciton-photon coupled modes with V polarization in the film with $d = 200$ nm, which are shown in Fig. 5(b), and the modes with H polarization are shown in Fig. 5(c). The dashed lines represent the dispersion relation of exciton-polariton in bulk crystal, and the horizontal bars are the coupled modes in the thin film. The length of each bar represents the sum of radiative and nonradiative decay rates, and the center is the resonant frequency. Since the H-polarized modes includes the longitudinal components, there are also the exciton-like modes with longitudinal exciton energy. The higher frequency parts of the scattering spectra in Fig. 5(a) apparently reflect the structure of the coupled modes shown in Figs. 5(b) and 5(c), and the peaks in lower frequency part appear satisfying the energy conservation. In this way, the scattering spectra of thin films are qualitatively different from the bulk one, and they depend on the film thickness, surroundings, and in-plane wave number obeying the change of exciton-photon coupled modes as discussed in Ref. 18. Furthermore, in contrast to the spectra for bulk crystal in Fig. 4, the emission near the exciton resonance $\omega \simeq \omega_{\rm T}$ can go outside the film, because of the large radiative decay rate in the thin film. From these results, the measurement of scattering spectra of RHPS can be considered a powerful tool[34] to observe the exciton-photon coupled modes in nanostructured materials in addition to the previously performed nonlinear optical experiments.[17,33]

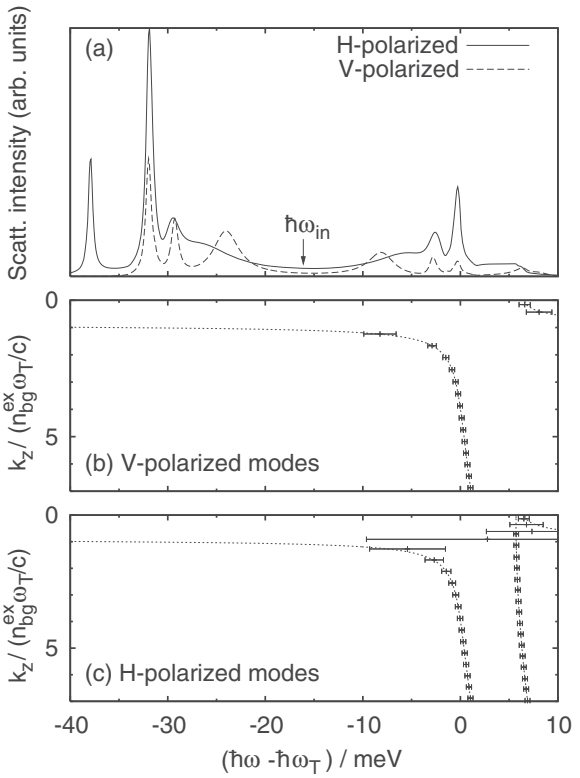

FIG. 5. (a) Polarization-resolved scattering spectra for thickness $d = 200$ nm and scattering angle $\theta = 60^\circ$. The film exists in vacuum and the pump frequency is tuned to resonantly excite the $m = 6$ biexciton state. (b) Dashed lines are the exciton-polariton dispersion relation in bulk crystal. The horizontal bars represent the exciton-photon coupled modes with V polarization in the film with $d =$ 200 nm. The bar length is the sum of radiative and nonradiative decay rates and the center is the resonance frequency. (c) The H-polarized modes are plotted. Because of the breaking of translational invariance in the z direction and the nonzero scattering angle, the longitudinal excitons are also optically allowed.

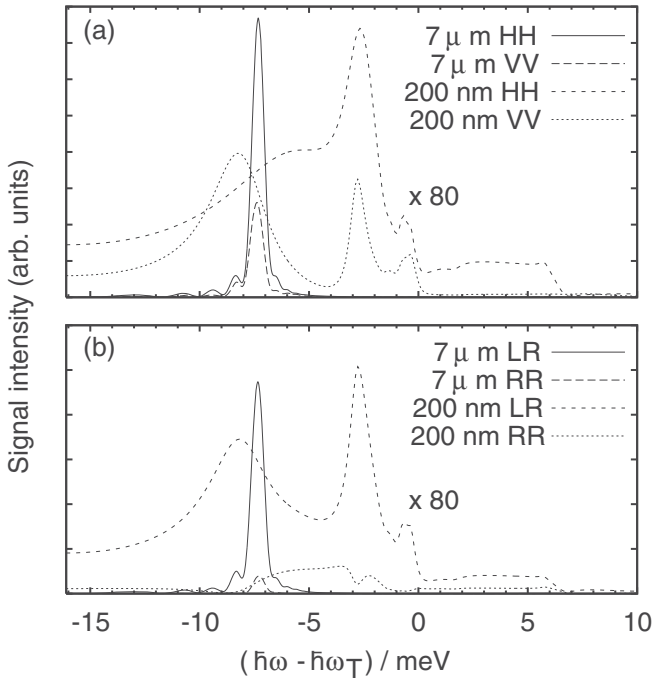

FIG. 6. The two-photon coincidence (signal) intensity is plotted as a function of scattering frequency ω of one of emitted photons. The spectra are resolved by the polarization of the two photons. CuCl films with thicknesses $d = 7$ μm and 200 nm are considered, and the scattering angle is $\theta = 60^\circ$. The same pump power is supposed for both thicknesses. (a) The polarization directions of two photons are resolved in H and V axes. The collinear pairs (HH and VV) are correlated, and the cross-linear pairs (HV and VH) are not generated from the lowest biexciton level in a film. (b) The polarization directions are resolved for circular polarization basis. Not only the pairs of left (L) and right (R) circularly polarizations are obtained, but LL and RR pairs are also generated for $\theta > 0$. The spectra of LR and RL are the same, and those of RR and LL are also the same. The spectra of 200 nm are magnified by factor 80 in both (a) and (b). Since the spectra are symmetrical about $\omega_{\rm in}$, only the high-frequency side $\omega > \omega_{\rm in}$ is shown.

B. Entangled-photon generation

Next, we discuss the entangled-photon generation by RHPS. Figure 6 shows polarization-resolved spectra of two-photon coincidence measurement. We plot only the signal intensity $C^{(2)S}_{\xi_1,\xi_2,\bar{k}_{\rm in}=0,\bar{k}_1=(\omega_T/c)\sin\theta}(z_1 > d, z_2 > d, \omega_{\rm in}, \omega)$ as a function of scattering frequency ω of a photon (the other photon has frequency of $2\omega_{\rm in} - \omega$). In Fig. 6(a), the pairs with $\xi_1 = \xi_2 = H$ and $\xi_1 = \xi_2 = V$ are considered, and the cross-linear pairs (HV and VH) have no correlation, because the photons are emitted from the lowest biexciton level with zero angular momentum. Two film thicknesses 7μm and 200 nm are considered, and the parameters are the same as in Figs. 4 and 5, respectively. In the two calculations, we considered the same pump power. Since the spectra are symmetrical about $\omega_{\rm in}$, we show only the high-frequency part $\omega > \omega_{\rm in}$. While similar as the scattering spectra in Fig. 4, the signal intensities of HH and of VV are not the same in general, when the scattering angle is nonzero. Therefore, the ideal entanglement in Eq. (25b) is not generally obtained, and the entangled state also has RR and LL components, whose spectra are shown in Fig. 6(b). Although this is a general property of bulk crystals, the situation is different in the case of the nano-to-bulk crossover regime. As seen in Fig. 6(a), we can obtain the same signal intensities for HH and VV at frequencies $\hbar\omega - \hbar\omega_{\rm T} = -9.8$ and -7.7 meV for $d = 200$ nm, and the signal intensities of RR and LL become nearly zero at frequency -8.8 meV in Fig. 6(b), while it is slightly different from the peak frequency -8.2 meV of the LR spectrum. These results mean that the state of emitted photon pairs can be modified by tuning the film thickness, scattering angle, and scattering frequency in the case of thin films. For example, at frequency -8.8 meV for $d = 200$ nm, we can get the entangled state $(|LR\rangle + |RL\rangle)/\sqrt{2}$, while the proportions of $|HH\rangle$ and $|VV\rangle$ components are not equal as seen in Fig. 6(a), because the polarization bases of the two photons are different for $\theta \neq 0$. On the other hand, at frequencies -9.8 and -7.7 meV, we get the entangled pairs with the same HH and VV proportions, while they contains RR and LL components.

Furthermore, even if the scattering angle is $\theta = 0^\circ$, in contrast to the bulk case, the scattering peaks are not at $\omega = \omega_{\rm T}$ in general in the case of thin films. Therefore, the maximally

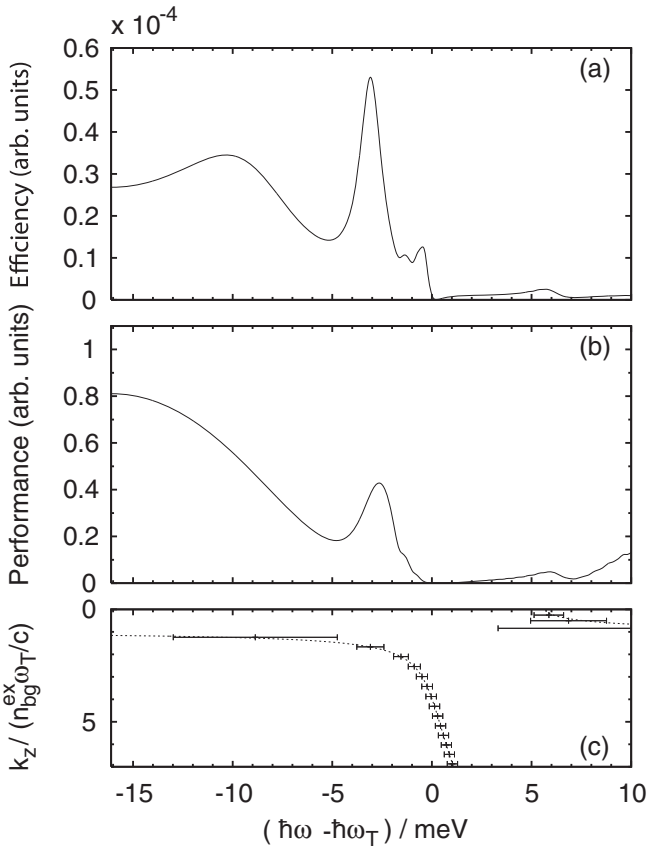

FIG. 7. (a) The generation efficiency (signal intensity) from a CuCl film with thickness $d = 200$ nm is plotted as a function of scattering frequency ω. The biexciton state $m = 6$ is resonantly excited, and the scattering angle is $\theta = 0^\circ$. (b) The spectrum of the corresponding performance P. The generation efficiency and the performance are normalized in the same manner as in Fig. 8. (c) The exciton-photon coupled modes for $\theta = 0^\circ$ in the film are plotted, while $\theta = 60^\circ$ in Fig. 5(b).

entangled photon pairs are obtained by frequency filtering for the emission at $\theta = 0^\circ$. Figure 7(a) shows the spectrum of signal intensity (generation efficiency) obtained by a CuCl film with thickness $d = 200$ nm for scattering angle $\theta = 0^\circ$. The proportions of HH and VV are the same, and RL and LR pairs are not emitted. As seen in Fig. 7(a), the peaks appear not at $\omega = \omega_{\rm in}$ but close to the resonance frequencies of the exciton-photon coupled modes shown in Fig. 7(c) (but not just at the resonance frequency because we get strong absorption near the exciton resonance frequency $\omega_{\rm T}$). In this way, compared to bulk crystals[10,13] and also to simple quantum dots,[4,5,7] the nano-to-bulk crossover regime has a variety of degrees of freedom to control the generated entangled state.

For the high-power generation of the entangled photons, the important factors are the generation efficiency and also the statistical accuracy, i.e., the number of unentangled pairs. For a pump beam with power $I_{\rm in}$, the signal intensity $S \propto C^{(2)\rm S}$ (amount of entangled pairs) is proportional to ${I_{\rm in}}^2$, while the noise intensity $N \propto C^{(2)\rm N}$ (amount of unentangled pairs) is proportional to ${I_{\rm in}}^4$, because an unentangled pair involves two biexcitons. This implies that by increasing the pump power $I_{\rm in}$, the S/N ratio decreases in contrast to the increase of S.[13]

To evaluate the material potential for the generation of strong and qualified entangled-photon beams, we introduce another measure termed "performance," P, defined as the signal intensity S under a certain S/N ratio α ($I_{\rm in}$ is tuned to give this ratio). This quantity $P = S^2/\alpha N$ does not depend on $I_{\rm in}$ and reflects the material potential. Figure 7(b) shows the spectrum of the performance. The exciton-photon coupled modes are shown in Fig. 7(c), and we can find that they govern the spectra of S of P. However, since the spectrum of the noise (product of scattering intensities) is different from the signal one, Figs. 7(a) and 7(b) are slightly different. The most significant difference is the spectra around $\omega = \omega_{\rm in} \sim \omega_{\rm T} - 16.1$ meV. While both S and P mostly reflect the resonance frequency of the exciton-photon coupled modes, the performance is maximized at $\omega = \omega_{\rm in}$, because P is strongly affected by nonradiative damping, which is smallest at that frequency.

Figure 8 shows thickness dependencies of (a) generation efficiency $S/{I_{\rm in}}^2$ and (b) performance P. The shapes of P curves do not depend on the choice of α, and the maximum value is normalized to unity. We also plot the generation efficiency with arbitrary units, because the estimation of absolute signal intensities are sensitive to the change of measurement conditions, while the spectral shape and thickness dependence do not depend on them. For simplicity, we assume that the two scattering fields are forward and perpendicular to the film ($\theta = 0^\circ$) and the frequencies are $\omega_{1/2} = \omega_{\rm in} \pm 0^+$. The pump frequency is tuned to the two-photon absorption in bulk material. The results for nonradiative decay rates $\gamma_{\rm ex} = 0, 0.1,$

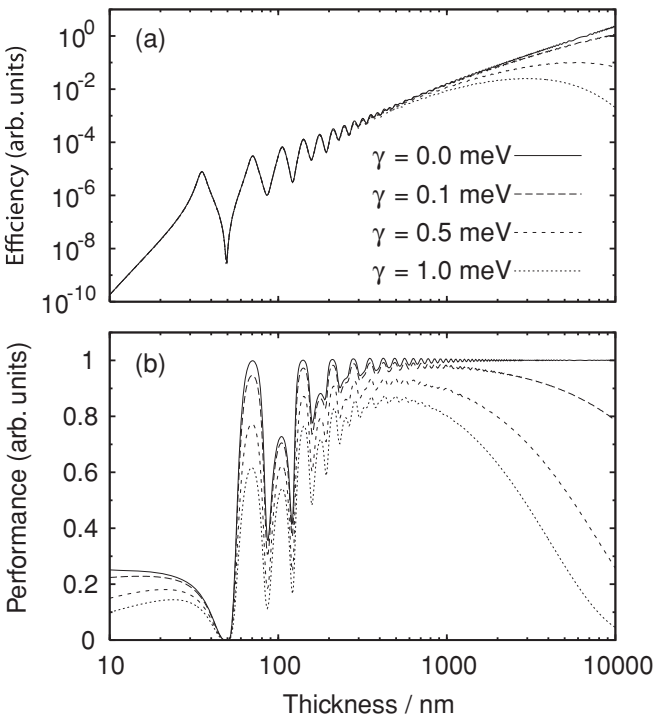

FIG. 8. Thickness dependencies of (a) generation efficiency $S/{I_{\rm in}}^2$ and (b) performance P. The scattering angle is $\theta = 0^\circ$ and the frequencies are $\omega_{1/2} = \omega_{\rm in} \pm 0^+$. To suppress the interference effect, outside medium is a dielectrics with $\varepsilon_{\rm bg}^{\rm ex}$. The results for $\gamma_{\rm ex} = 0, 0.1,$ 0.5, and 1.0 meV are plotted with different lines. The performance is normalized to the ideal quantity.

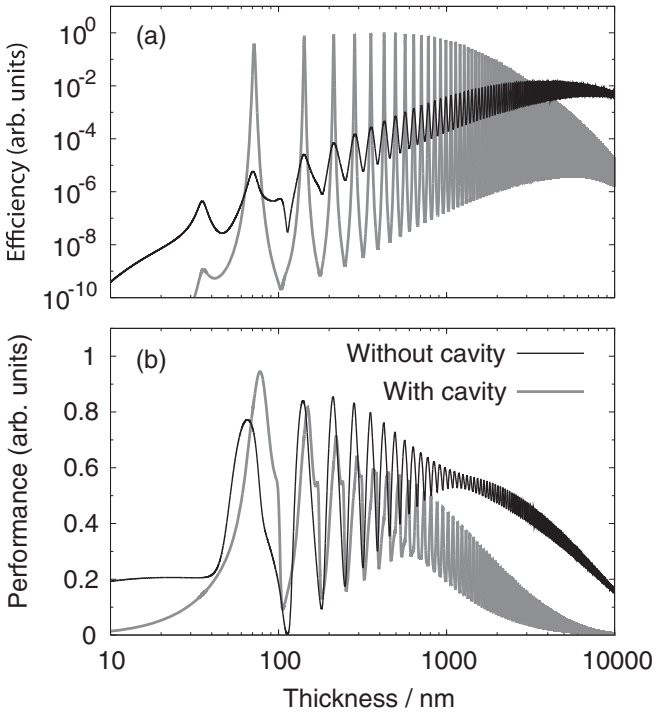

FIG. 9. Thickness dependencies of (a) generation efficiency $S/I_{\rm in}{}^2$ and (b) performance P. The black lines represent the results for a bare CuCl film existing in vacuum. The scattering frequencies are $\omega_{1/2} = \omega_{\rm in} \pm 0^+$, and the angle is $\theta = 0^\circ$ (forward). The gray lines represent the results for DBR cavity embedding a CuCl layer shown in Fig. 2(b). The mode frequency of the optical cavity is tuned to $\omega_{\rm T}$, and the scattering is backward with $\theta = 180^\circ$. In both cases, $\gamma_{\rm ex} = 0.5$ meV. The performance is normalized in the same manner as in Fig. 8.

0.5, and 1.0 meV are plotted with different lines. In order to suppress the oscillation due to the interference as seen in Fig. 3, we suppose that the CuCl film exists in a dielectric medium with $\varepsilon_{\rm bg}^{\rm ex}$. The results for the film in vacuum are shown in Fig. 9. In Fig. 8, the oscillating behavior in the nanometer thickness range is due to the biexciton confinement and the modification of the energy structure of exciton-photon coupled modes. The RHPS effectively occurs when the resonance energy of the coupled mode is just equal to half the biexciton energy. The maximum performance shown in Fig. 8(b) is the ideal quantity, and it depends on measurement conditions, such as resolutions of angle and frequency, but not on material parameters.

As seen in Fig. 8(a) and also in Ref. 12, the optimal thickness for generation efficiency is determined by $\gamma_{\rm ex}$, and it is on the order of micrometers or more for CuCl crystals. However, as seen in Fig. 8(b), the performance significantly decreases from the ideal value at thickness of micrometers for nonzero $\gamma_{\rm ex}$, because the nonradiative decay easily increases the amount of unentangled pairs. Therefore, when we use bulk crystals, the generation efficiency (generation probability for one pump pulse) is limited by desired statistical accuracy (S/N ratio).[13] However, at thickness from 50 to 1000 nm, as expected, nearly the ideal performance can be obtained at particular thicknesses even if $\gamma_{\rm ex}$ is nonzero. This is because the radiative decay is dominant owing to the exciton superradiance in the nano-to-bulk crossover regime,[17,18] and the entangled pairs can go outside the film without decreasing the amplitude. Therefore, thin films generally show a high performance, and this rapid decay is also desired for the high-repetition excitation, which also recovers the signal intensity while maintaining the S/N ratio.[13]

C. With DBR cavity

Although a good performance is obtained at a thickness of hundreds of nanometers, the generation efficiency of such thin films is much lower than that of bulk crystals as seen in Fig. 8(a), and a strong pump power is required to obtain a sufficient signal intensity at such thickness range. While the superradiant excitons maintain the large nonlinearity (excitonic component),[17] this low efficiency simply comes from the small thickness (interaction volume). This problem can be overcome by using an optical cavity in the strong-coupling regime, because we can control both the interaction volume and radiative decay rate using two parameters: quality factor (Q factor) of cavity and thickness of CuCl. This aspect is different from simple semiconductor microcavities, in which the interaction volume and radiative decay rate are respectively enhanced in strong- and weak-coupling regimes.

Although a high generation efficiency can be achieved by using a high-Q cavity, we have to simultaneously realize a rapid radiative decay of entangled photons inside the cavity. Therefore, we consider a low-Q cavity as reported in Ref. 69, namely, a CuCl layer with DBRs consisting of PbF_2 and $PbBr_2$ as seen in Fig. 2(b). Here, since the translational invariance is broken at thickness of nanometers, the generated photons can go forward and also backward in contrast to the bulk case. Therefore, we suppose a high reflectance on the transmission side to suppress the leakage of entangled photons, and we focus on the backward emission. The DBR cavity is considered by the background dielectric function $\varepsilon_{\rm bg}(\boldsymbol{r},\omega)$ in Eq. (9). The refractive indexes of PbF_2 and $PbBr_2$ are 1.86 and 2.95, respectively. The gray lines in Fig. 9 represent the backward emission from the cavity, where the cavity mode frequency is tuned to $\omega_{\rm T}$, $\gamma_{\rm ex} = 0.5$ meV, and the periods of the incident and transmitted sides are 4 and 16, respectively (Q factor is 50). This system corresponds to the weak bipolariton regime[15,16] (but the strong-coupling regime of excitons and photons), where the energy splitting between polariton and biexciton levels is small compared to their broadening. This situation is in contrast to those in Refs. 15 and 16, where the strong enhancement of entangled-photon generation from a quantum well in a high-Q cavity has been discussed on the basis of the biexcitonic cavity-QED picture or the strong bipolariton picture. As shown in Fig. 9(a), since biexcitons are effectively created, the generation efficiency is significantly enhanced at thickness range of nanometers, and it is larger than the maximum value by bare CuCl film existing in vacuum (black line). The enhancement also occurs when the polariton energy (exciton-photon coupled mode) is equal to half the biexciton energy, which is consistent with the results in Refs. 15 and 16. Compared with Fig 8(a), the period of the oscillation is doubled, because the RHPS involving biexcitons with odd-parity center-of-mass motion is forbidden in the one-sided optical cavity. On the other hand, as shown in Fig. 9(b), at thicknesses of micrometers,

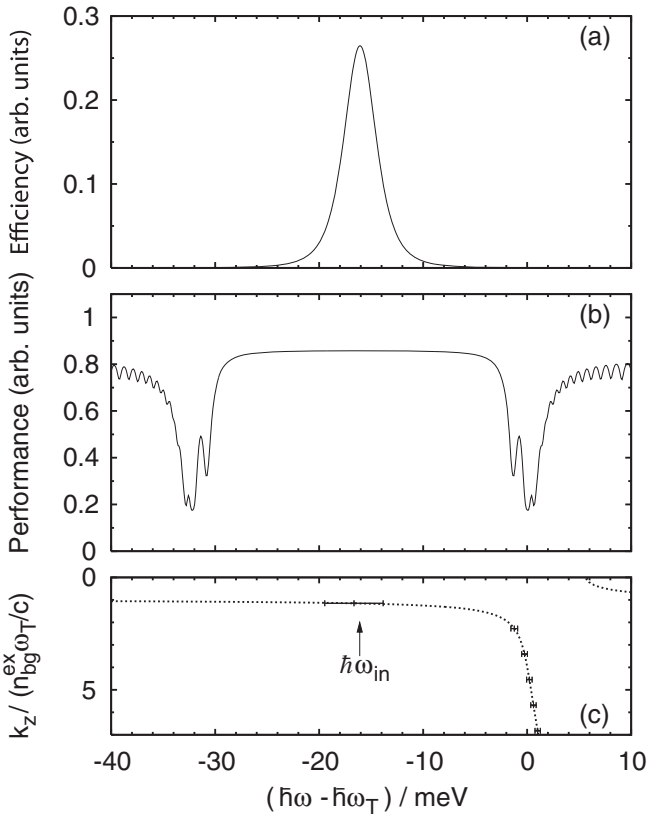

FIG. 10. (a) The generation efficiency (signal intensity) is plotted as a function of scattering frequency ω. A CuCl film with thickness $d = 72$ nm is embedded in the DBR cavity considered in Fig. 9, and the other parameters are also the same. (b) The spectrum of the corresponding performance P. (c) The exciton-photon coupled modes in the film are plotted in the same manner as in Fig. 5(b).

the performance is suppressed compared with that of the bare CuCl film. This is because of the multiple reflections inside the cavity, and the scattered fields nonradiatively decay during the propagation. In contrast, at thicknesses of nanometers, particularly at 80 nm, the performance almost maintains the ideal quantity. This is due to the enhancement of the radiative decay rate by exciton superradiance, and the enhancement of generation efficiency is simultaneously obtained by the cavity effect in the strong-coupling regime.

Finally, in Figs. 10(a) and 10(b), we show the spectra of generation efficiency and performance, respectively, in the case of CuCl film with thickness $d = 72$ nm embedded in the DBR cavity discussed above. This thickness is chosen to achieve a high generation efficiency, while the performance at $\omega = \omega_{in}$ is 0.86, which is smaller than the maximum value in Fig. 9(b). However, compared to thin films without the cavity, the generation efficiency is significantly increased and the high performance is successfully maintained due to the rapid radiative decay. Further, while the pump frequency ω_{in} is assumed to the two-photon absorption frequency in bulk CuCl in Figs. 10(a) and 10(b), we have numerically checked that when ω_{in} is correctly tuned to the eigen frequency of a confined biexciton mode, the generation efficiency is enhanced more dramatically while maintaining the high performance.

In Fig. 10(c), the exciton-photon coupled modes are plotted with horizontal bars, and we can find that one mode with high radiative decay rate exists close to the pump frequency ω_{in} (two-photon absorption frequency of biexcitons). This mode corresponds to the lower cavity polariton, and the strong electric field in the cavity enhances the generation efficiency of biexcitons due to the cavity-induced double resonance.[70] Furthermore, the generated entangled excitons rapidly decay into photons through this polariton mode, which ensures the high performance by the same material structure and pump conditions.

In this way, by using an optical cavity embedding a CuCl layer with a thickness of nanometers, we can obtain a high efficiency and a high performance simultaneously. To avoid the leakage of generated photons, the reflectance on the transmission side should be high enough, but that on the incident side should not be high to obtain a rapid radiative decay rate. Once we choose a cavity structure, we can numerically determine the optimal thickness of the CuCl layer, in which an exciton-photon coupled mode has half the biexciton frequency, a rapid radiative decay rate, and also large exciton component (large nonlinearity) to achieve a high performance and a high generation efficiency. Such a coupled mode is a unique feature in the nano-to-bulk crossover regime.

V. SUMMARY

We have developed a theoretical framework for the investigation of biexciton-RHPS based on the QED theory for excitons.[44] Compared to the previous theories,[12,39] our method can be applied to the nano-to-bulk crossover regime, because the center-of-mass motions of excitons and biexcitons are explicitly considered. Further, we can discuss the polarization correlation of entangled pairs and also surroundings of the excitonic layer, such as the DBR cavity structure. While we considered CuCl films in actual calculation, by treating several relative exciton levels and by correctly calculating the center-of-mass wave functions of excitons confined in finite crystal including the effect of a dead layer,[71] our theoretical framework can be applied to other materials in principle. Further, by correctly treating the modification of relative motion of excitons and biexcitons strongly confined in nanocrystals and also the Pauli exclusion principle, our framework can be extended for the investigation of a single quantum dot and the deterministic generation of entangled photons.

We have calculated the scattering spectra of RHPS from CuCl films with bulklike and submicron thicknesses. At the bulklike thickness, the four peaks called M_T, M_L, LEP, and HEP are reproduced as observed in experiments. On the other hand, scattering spectra of the thin film are significantly modified from the bulk ones, reflecting the exciton-photon coupled modes in the thin film.[17,18,21,33,35] In other words, the RHPS measurement is also useful to observe the exciton-photon coupled modes in nanostructured materials[34] as well as the four-wave mixing[17,29,35] and the two-photon excitation scattering.[33]

In addition to the signal intensity of entangled-photon generation, we also discuss the performance of material structures by considering the noise intensity originating from

two independent biexcitons. Although the signal intensity is maximized at a thickness of micrometers,[12,39] a high performance is obtained at a thickness of nanometers due to the rapid radiative decay of excitons. However, the generation efficiency of such thin films is weaker than the bulk one in general. We have demonstrated that by using a DBR cavity embedding an excitonic layer in the nano-to-bulk crossover regime, the generation efficiency can be enhanced while maintaining a high performance.

For the pursuit of high-power and high-quality but probabilistic generation of entangled photons, which is essential for the next-generation technologies of fabrication and chemical reaction,[9] the biexciton-RHPS shows a high generation efficiency compared to the PDC one. From the viewpoint of the quality of generated entangled pairs, by implementing a DBR cavity embedding a CuCl nanolayer, the RHPS can show a high performance while maintaining high efficiency. Such a structure has also a variety of degrees of freedom to control the generated states of entangled photons. We believe that our results make a breakthrough in high-power and high-quality entangled-photon generation.

ACKNOWLEDGMENTS

The authors are grateful to K. Edamatsu, G. Oohata, H. Ajiki, and H. Oka for helpful discussions. This work was partially supported by the Japan Society for the Promotion of Science (JSPS): a Grant-in-Aid for Creative Science Research 17GS1204 (2005), Grant-in-Aid for Scientific Research (B) 21340085, and Grant No. 19-997.

*Present address: Laboratoire Matériaux et Phénomènes Quantiques, Université Paris Diderot-Paris 7 et CNRS, Case 7021, Bâtiment Condorcet, F-75013 Paris, France, motoaki.bamba@univ-paris-diderot.fr

[1] A. Einstein, B. Podolsky, and N. Rosen, Phys. Rev. **47**, 777 (1935).
[2] P. G. Kwiat, K. Mattle, H. Weinfurter, A. Zeilinger, A. V. Sergienko, and Y. Shih, Phys. Rev. Lett. **75**, 4337 (1995).
[3] P. G. Kwiat, E. Waks, A. G. White, I. Appelbaum, and P. H. Eberhard, Phys. Rev. A **60**, R773 (1999).
[4] N. Akopian, N. H. Lindner, E. Poem, Y. Berlatzky, J. Avron, D. Gershoni, B. D. Gerardot, and P. M. Petroff, Phys. Rev. Lett. **96**, 130501 (2006).
[5] R. M. Stevenson, R. J. Young, P. Atkinson, K. Cooper, D. A. Ritchie, and A. J. Shields, Nature (London) **439**, 179 (2006).
[6] R. J. Young, R. M. Stevenson, A. J. Hudson, C. A. Nicoll, D. A. Ritchie, and A. J. Shields, Phys. Rev. Lett. **102**, 030406 (2009).
[7] C. L. Salter, R. M. Stevenson, I. Farrer, C. A. Nicoll, D. A. Ritchie, and A. J. Shields, Nature (London) **465**, 594 (2010).
[8] A. Dousse, J. Suffczynski, A. Beveratos, O. Krebs, A. Lemaitre, I. Sagnes, J. Bloch, P. Voisin, and P. Senellart, Nature (London) **466**, 217 (2010).
[9] Y. Kawabe, H. Fujiwara, R. Okamoto, K. Sasaki, and S. Takeuchi, Opt. Express **15**, 14244 (2007).
[10] K. Edamatsu, G. Oohata, R. Shimizu, and T. Itoh, Nature (London) **431**, 167 (2004).
[11] M. Ueta, H. Kanzaki, K. Kobayashi, Y. Toyozawa, and E. Hanamura, *Excitonic Processes in Solids* (Springer-Verlag, Berlin, 1986).
[12] S. Savasta, G. Martino, and R. Girlanda, Solid State Commun. **111**, 495 (1999).
[13] G. Oohata, R. Shimizu, and K. Edamatsu, Phys. Rev. Lett. **98**, 140503 (2007).
[14] M. Bamba and H. Ishihara, Phys. Rev. Lett. **105**, 123906 (2010).
[15] H. Ajiki and H. Ishihara, J. Phys. Soc. Jpn. **76**, 053401 (2007).
[16] H. Oka and H. Ishihara, Phys. Rev. Lett. **100**, 170505 (2008).
[17] M. Ichimiya, M. Ashida, H. Yasuda, H. Ishihara, and T. Itoh, Phys. Rev. Lett. **103**, 257401 (2009).
[18] M. Bamba and H. Ishihara, Phys. Rev. B **80**, 125319 (2009).
[19] A. Tredicucci, Y. Chen, F. Bassani, J. Massies, C. Deparis, and G. Neu, Phys. Rev. B **47**, 10348 (1993).
[20] Z. K. Tang, A. Yanase, Y. Segawa, N. Matsuura, and K. Cho, Phys. Rev. B **52**, 2640 (1995).
[21] M. Bamba and H. Ishihara, J. Phys. Soc. Jpn. **78**, 043701 (2009).
[22] J. Knoester, Phys. Rev. Lett. **68**, 654 (1992).
[23] G. Björk, S. Pau, J. M. Jacobson, H. Cao, and Y. Yamamoto, Phys. Rev. B **52**, 17310 (1995).
[24] V. M. Agranovich, D. M. Basko, and O. A. Dubovsky, J. Chem. Phys. **106**, 3896 (1997).
[25] H. Ajiki, J. Lumin. **94-95**, 173 (2001).
[26] H. Ishihara and K. Cho, Phys. Rev. B **53**, 15823 (1996).
[27] K. Akiyama, N. Tomita, Y. Nomura, and T. Isu, Appl. Phys. Lett. **75**, 475 (1999).
[28] H. Ishihara, T. Amakata, and K. Cho, Phys. Rev. B **65**, 035305 (2001).
[29] H. Ishihara, K. Cho, K. Akiyama, N. Tomita, Y. Nomura, and T. Isu, Phys. Rev. Lett. **89**, 017402 (2002).
[30] K. Cho, *Optical Response of Nanostructures: Microscopic Nonlocal Theory* (Springer-Verlag, Berlin, 2003).
[31] H. Ishihara, Phys. Rev. B **67**, 113302 (2003).
[32] H. Ishihara, J. Kishimoto, and K. Sugihara, J. Lumin. **108**, 343 (2004).
[33] A. Syouji, B. P. Zhang, Y. Segawa, J. Kishimoto, H. Ishihara, and K. Cho, Phys. Rev. Lett. **92**, 257401 (2004).
[34] H. Ishihara, A. Syouji, Y. Segawa, and M. Bamba, J. Phys. Condens. Matter **19**, 445008 (2007).
[35] O. Kojima, T. Isu, J. Ishi-Hayase, A. Kanno, R. Katouf, M. Sasaki, and M. Tsuchiya, J. Phys. Soc. Jpn. **77**, 044701 (2008).
[36] H. Yasuda and H. Ishihara, Phys. Rev. B **79**, 193308 (2009).
[37] M. Inoue and E. Hanamura, J. Phys. Soc. Jpn. **41**, 1273 (1976).
[38] E. Hanamura and T. Takagahara, J. Phys. Soc. Jpn. **47**, 410 (1979).
[39] S. Savasta and R. Girlanda, Phys. Rev. B **59**, 15409 (1999).
[40] B. Huttner and S. M. Barnett, Phys. Rev. A **46**, 4306 (1992).
[41] L. Knöll, S. Scheel, and D.-G. Welsch, in *Coherence and Statistics of Photons and Atoms*, edited by J. Peřina (Wiley, New York, 2001), Chap. 1, pp. 1–64.
[42] T. Östreich, K. Schonhammer, and L. J. Sham, Phys. Rev. Lett. **74**, 4698 (1995).
[43] T. Östreich, K. Schonhammer, and L. J. Sham, Phys. Rev. B **58**, 12920 (1998).
[44] M. Bamba and H. Ishihara, Phys. Rev. B **78**, 085109 (2008).

[45]K. Cho, Prog. Theor. Phys. Suppl. **106**, 225 (1991).
[46]K. Cho, J. Phys. Soc. Jpn. **55**, 4113 (1986).
[47]T. Itoh, T. Suzuki, and M. Ueta, J. Phys. Soc. Jpn. **42**, 1069 (1977).
[48]T. Itoh and T. Suzuki, J. Phys. Soc. Jpn. **45**, 1939 (1978).
[49]M. Ueta, T. Mita, and T. Itoh, Solid State Commun. **32**, 43 (1979).
[50]T. Mita, K. Sôtome, and M. Ueta, J. Phys. Soc. Jpn. **48**, 496 (1980).
[51]T. Mita, K. Sôtome, and M. Ueta, Solid State Commun. **33**, 1135 (1980).
[52]Y. Nozue, J. Phys. Soc. Jpn. **51**, 1840 (1982).
[53]H. Akiyama, T. Kuga, M. Matsuoka, and M. Kuwata-Gonokami, Phys. Rev. B **42**, 5621 (1990).
[54]E. Tokunaga, A. L. Ivanov, S. V. Nair, and Y. Masumoto, Phys. Rev. B **59**, R7837 (1999).
[55]A. L. Ivanov and H. Haug, Phys. Rev. B **48**, 1490 (1993).
[56]A. L. Ivanov, H. Haug, and L. V. Keldysh, Phys. Rep. **296**, 237 (1998).
[57]E. Tokunaga, A. L. Ivanov, S. V. Nair, and Y. Masumoto, J. Lumin. **87–89**, 216 (2000).
[58]E. Tokunaga, K. Kurihara, M. Baba, Y. Masumoto, and M. Matsuoka, Phys. Rev. B **64**, 045209 (2001).
[59]R. Matloob, R. Loudon, S. M. Barnett, and J. Jeffers, Phys. Rev. A **52**, 4823 (1995).
[60]S. Savasta and R. Girlanda, Phys. Rev. A **53**, 2716 (1996).
[61]T. Gruner and D.-G. Welsch, Phys. Rev. A **54**, 1661 (1996).
[62]S. Savasta, O. D. Stefano, and R. Girlanda, J. Opt. Soc. Am. B **19**, 304 (2002).
[63]M. Khanbekyan, L. Knöll, and D.-G. Welsch, Phys. Rev. A **67**, 063812 (2003).
[64]L. G. Suttorp and M. Wubs, Phys. Rev. A **70**, 013816 (2004).
[65]J. Singh, Phys. Solid State **40**, 728 (1998).
[66]N. Matsuura and K. Cho, J. Phys. Soc. Jpn. **64**, 651 (1995).
[67]W. C. Chew, *Waves and Fields in Inhomogeneous Media* (IEEE, New York, 1995).
[68]A. A. Abrikosov, L. P. Gorkov, and I. E. Dzyaloshinski, *Methods of Quantum Field Theory in Statistical Physics* (Dover, New York, 1975), Chap. 6.
[69]G. Oohata, T. Nishioka, D. Kim, H. Ishihara, and M. Nakayama, Phys. Rev. B **78**, 233304 (2008).
[70]H. Ishihara and K. Cho, Appl. Phys. Lett. **71**, 3036 (1997).
[71]V. M. Agranovich and V. L. Ginzburg, *Crystal Optics with Spatial Dispersion, and Excitons* (Springer-Verlag, Berlin, 1984).